CORE
Metadata, citation and similar papers at core.ac.uk
Provided by Digital Repository at the University of Maryland

ABSTRACT

Title of Document: TRACING SULFUR SOURCES IN AN ARCHEAN HYDROTHERMAL SYSTEM USING SULFUR MULTIPLE ISOTOPES – A CASE STUDY FROM THE KIDD CREEK VOLCANOGENIC MASSIVE SULFIDE DEPOSIT

John William Jamieson, M.S., 2005

Directed By: Professor James Farquhar
Department of Geology

Mass-independent fractionation of sulfur isotopes in the Archean atmosphere resulted in surface sulfur reservoirs with distinct isotopic signatures. These signatures are used to trace the movement of sulfur through an Archean seafloor hydrothermal system associated with the Kidd Creek volcanogenic massive sulfide (VMS) deposit. Isotopic measurements of sulfides from the 2.7 Ga Kidd Creek VMS deposit reflect two separate sulfur sources for ore precipitation. Subseafloor ore has a predominantly juvenile sulfur source. with a small (~3%) component of seawater sulfate, which was transported through the hydrothermal system to the site of precipitation. Surface sulfides contain a significant proportion of sulfur that was stripped from coeval seawater sulfate or native sulfur at the site of precipitation. Mass-independent isotopic signatures are also used in a sulfur multiple-isotope framework to evaluate isotopic disequilibrium and to assess the suitability of mineral pairs for paleothermometric calculations in the Kidd Creek VMS deposit.

TRACING SULFUR SOURCES IN AN ARCHEAN HYDROTHERMAL SYSTEM USING SULFUR MULTIPLE ISOTOPES – A CASE STUDY FROM THE KIDD CREEK VOLCANOGENIC MASSIVE SULFIDE DEPOSIT

By

John William Jamieson

Thesis submitted to the Faculty of the Graduate School of the
University of Maryland, College Park, in partial fulfillment
of the requirements for the degree of
Master of Science
2005

Advisory Committee:
Professor James Farquhar, Chair
Professor Philip A. Candela
Professor A. Jay Kaufman

Acknowledgements

I would like to thank James Farquhar for giving me the opportunity to come to Maryland and allowing me to pursue such interesting research topics. This thesis has benefited immensely from his wisdom and open mind. I would like to thank Boswell Wing for his guiding hand throughout this project. Without his scientific, technical and moral support, the potential of this research would not have been realized. Daily laboratory discussions with James, Boz, and David Johnston, together with their infinite sense of humor, made working in the lab a pleasure. Discussions with Mark Hannington and Ian Jonasson greatly improved my understanding of the geology of the Kidd Creek region. Comments and suggestions by Philip Candela and Jay Kaufman have enhanced the quality of this thesis.

Finally, I would like to especially thank Anetta Banas for her endless love, emotional support and scientific insights, all of which have kept me close to home.

This research was supported by an NSERC Post-Graduate Scholarship to J.W. Jamieson, NSF grants EAR-0348382 and EAR-0003419 to J. Farquhar, and NASA Exobiology grant NAG-512350 to J. Farquhar and B.A. Wing.

Table of Contents

List of Tables

List of Figures

Chapter 1: Introduction

1.1 Overview

Reports of mass-independent sulfur isotope signatures in Archean sedimentary rocks (Farquhar et al., 2000; 2001) have yielded significant new insights into the Earth's early sulfur cycle and its ties to the chemistry of the Archean atmosphere. The results of the research by Farquhar et al. (2000; 2001) have raised a number of questions about the size of Archean geochemical reservoirs and the vigor of exchange between them. One of the most poorly understood of these reservoirs is that of oceanic sulfate. Sulfate in Archean oceans is thought to have had a unique and characteristic mass-independent sulfur isotope signatures, and recent work (Wing et al., 2002) indicates that this signature is transferred to sulfide minerals in several Archean VMS (Volcanogenic Massive Sulfide) deposits in the Superior Province of Canada. Here, I focus on the Archean VMS deposit, Kidd Creek, located near Timmins, Ontario, to study the nature of the oceanic sulfate reservoir, and to extract new information about the nature of the hydrothermal systems and processes that operated during formation of Archean VMS deposits.

1.2 Mass-independent Fractionation

Sulfur isotope analyses are reported as δ values, which for ^{34}S and ^{32}S, are defined as:

$$\delta^{34}S_{Sample} = \left(\frac{^{34}R_{Sample}}{^{34}R_{V-CDT}} - 1 \right) \times 1000, \quad (1.1)$$

where ^{34}R is the ratio of the abundance of ^{34}S to abundance of ^{32}S, and the V-CDT subscript indicates the reference scale defined by the isotopic composition of the international standard Ag_2S, IAEA-S1. This standard has a defined isotopic composition of $\delta^{34}S \equiv -0.3$ ‰ V-CDT (Krouse and Coplen, 1997). Samples were measured relative to a laboratory standard SF_6 gas. This gas has a known composition, relative to the IAEA-S1 standard, based on multiple repeat measurements. For this study, we took IAEA-S1 to have $\delta^{33}S = -0.05$ per mil V-CDT (Gao and Thiemens, 1993), which assumes concordance between the CDT and V-CDT scales.

Isotope effects that accompany most chemical and physical processes are controlled by the relative difference in mass of the isotopes. Variations of $\delta^{33}S$ values are usually about half the coincident variations in $\delta^{34}S$ values and reflect the fact that $\delta^{33}S$ is a measure of changes in $^{33}S/^{32}S$ (1 a.m.u difference) and $\delta^{34}S$ is a measure of changes in $^{34}S/^{32}S$ (2 a.m.u. difference). This mass dependence of sulfur isotope fractionation produces a highly-correlated array on a plot of $\delta^{33}S$ versus $\delta^{34}S$ values for most terrestrial sulfur-bearing materials (Fig. 1). Theoretical calculations, based on equilibrium isotope partitioning, indicate that this array should be described by

$$\delta^{33}S = \left[\left(\frac{\delta^{34}S}{1000} + 1\right)^{\lambda} - 1\right] \times 1000, \quad (1.2)$$

with $\lambda = 0.515$ (+0.003/-0.002) (Hulston and Thode, 1965). Sulfur-bearing terrestrial samples that are older than ~2.45 Ga have been shown to possess sulfur multiple-isotope compositions that, in some cases, fall far outside the limits allowed by mass-dependent variations in λ (e.g., Farquhar et al., 2000). Precisely how a sample's

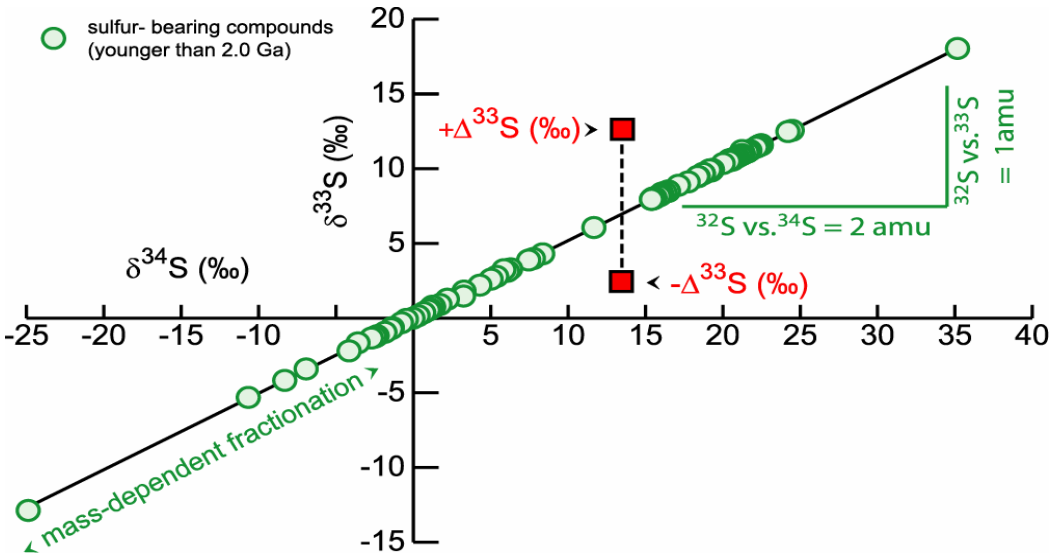

Figure 1: $\delta^{33}S$ vs. $\delta^{34}S$ plot of terrestrial, mass-dependent sulfur-bearing compounds younger than 2.0 Ga. The black line represents the Terrestrial Fractionation Line (TFL). The slope of this line (~0.5) reflects the 1 a.m.u difference recorded by $\delta^{33}S$, relative to the 2 a.m.u. difference recorded by $\delta^{34}S$. Sulfur-bearing samples that have experience mass-independent fractionation will plot above or below the TFL.

sulfur multiple-isotope composition deviates from a reference mass-dependent fractionation array can be quantified by the following relationship:

$$\Delta^{33}\mathrm{S} = \delta^{33}\mathrm{S} - \left[\left(\frac{\delta^{34}\mathrm{S}}{1000}+1\right)^{\lambda_{\mathrm{RFL}}} - 1\right] \times 1000\,, \quad (1.3)$$

where λ_{RFL} (Reference Fractionation Line) ≡ 0.515 (Hulston and Thode, 1965). This formulation removes much of the mass-dependent correlation that is inherent in the fractionation due to most chemical and physical isotope effects, and provides a measure to describe deviations from the RFL. In essence, it transforms $\delta^{33}S$ values into a new coordinate space where the exponential curve described by (1.2) is parallel to the $\delta^{34}S$ axis.

1.3 Archean Sulfur Cycle

Mass-independent fractionation of sulfur isotopes is recorded in natural samples older than 2.45 Ga (Fig. 2) (Farquhar et al., 2000; Farquhar and Wing, 2003;Mojzsis et al., 2003; Ono et al., 2003; Bekker et al., 2004). Samples that are younger than 2.0 Ga have $\Delta^{33}S$ values indicating no significant mass-independent fractionation. This shift in isotope fractionation mechanisms and/or preservation of isotope ratios in the rock record indicates a fundamental change in sulfur chemistry and/or cycling through the Earth system in the Neoarchean. The only experimentally verified mechanism for producing substantial non-zero $\Delta^{33}S$ values is through photochemistry of sulfur-bearing gas phase compounds (Thiemens, 1999; Farquhar et al., 2000; 2001).

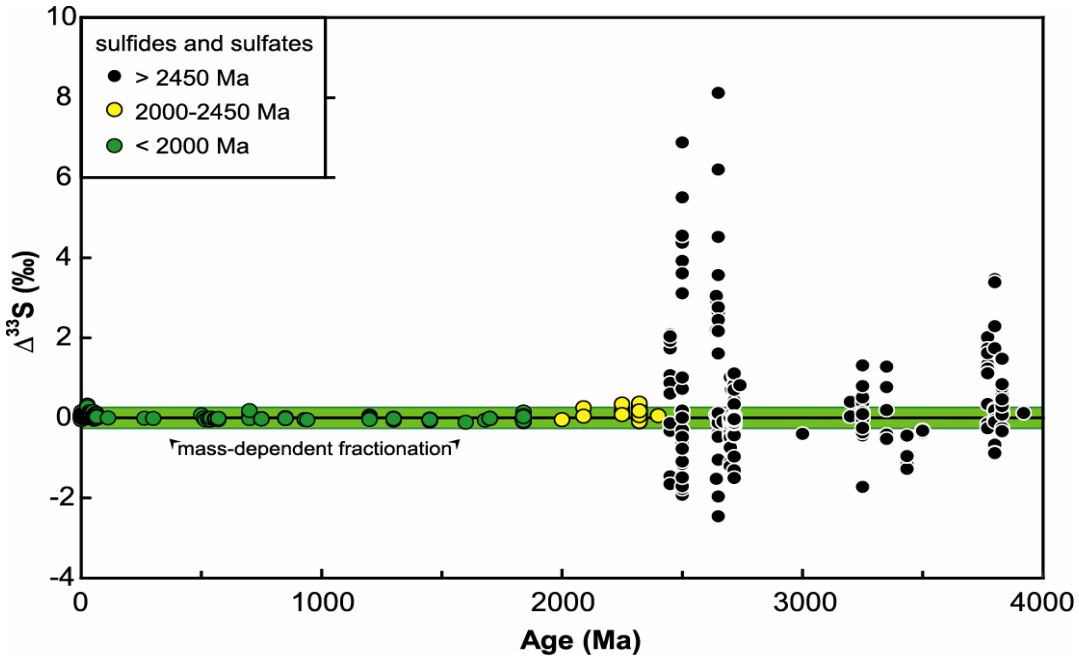

Figure 2: Plot of $\Delta^{33}S$ of terrestrial sulfur compounds versus time, showing mass-independent fractionation in samples older than 2.45 Ga. The green zone surrounding the x-axis indicates the deviations from the TFL that are permissible for mass-dependent processes. (Sources: Farquhar et al.; 2000, Mojzsis et al., 2003; Ono et al., 2003; Hu et al., 2003;Bekker et al., 2004; unpublished data from this lab)

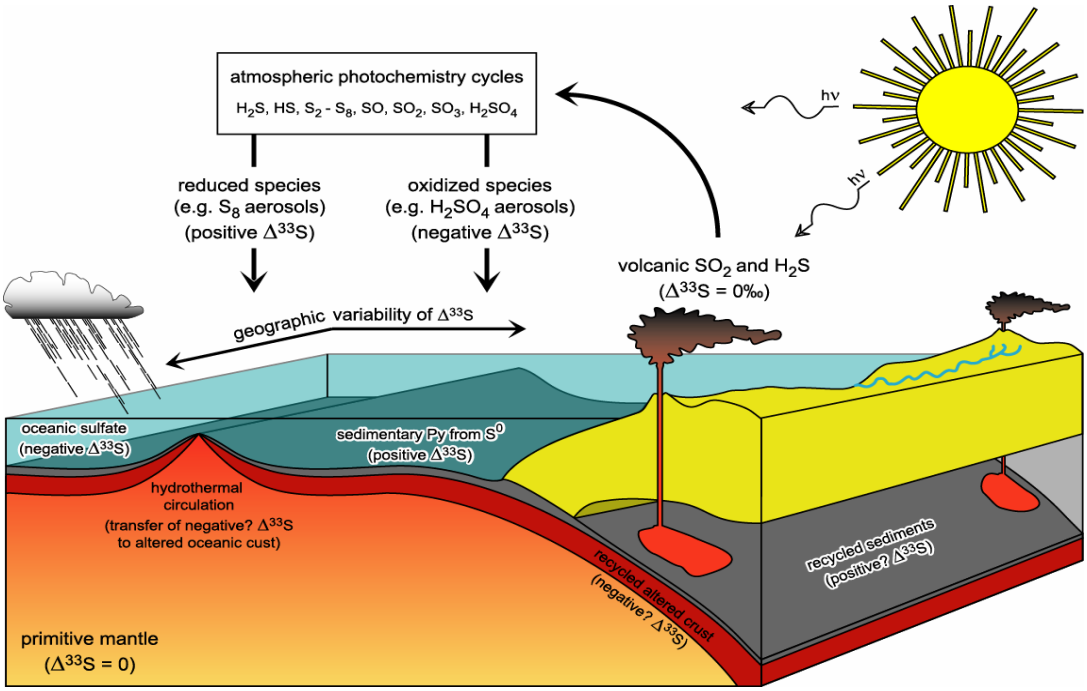

Figure 3: Conceptual diagram of the Archean sulfur cycle, showing the movement of various sulfur species between reservoirs and their associated $\Delta^{33}S$ values. Juvenile sulfur is erupted in to the atmosphere with an initial $\Delta^{33}S$ of 0‰. Photochemical reactions in the atmosphere impart non-zero $\Delta^{33}S$ values on intermediate sulfur species, which ultimately return to the surface in a soluble oxidized form (sulfate) and insoluble reduced form (S_8 aerosol), with negative and positive $\Delta^{33}S$ values, respectively. Modified from Farquhar and Wing (2003).

A variant of this mechanism has been incorporated into a model of the Archean sulfur cycle (Fig. 3). According to this model, sulfur from the mantle, with a $\Delta^{33}S$ value of 0 per mil, is erupted into the atmosphere as SO_2. These gaseous sulfur species undergo photochemical reactions in the presence of solar ultra-violet radiation, producing a number of intermediate chemical species. The ultimate sulfur-bearing products of these gas-phase reactions are oxidized sulfur species (sulfate), which leave the atmosphere with negative values of $\Delta^{33}S$, and reduced sulfur species (S_8 aerosols), which leave the atmosphere with positive $\Delta^{33}S$ values (Farquhar et al, 2001; Pavlov and Kasting, 2002). This dissociation reaction can be summarized as:

$$4S + 4H_2O = 3H_2S + H_2SO_4 \quad (1.4)$$

A low O_2 atmosphere is necessary for the production of non-zero $\Delta^{33}S$ values, because high O_2 levels will result in ozone shielding of UV radiation, inhibiting the photochemical reactions that produce mass-independent fractionations (Farquhar et al, 2001). Low O_2 levels are also necessary for the preservation of non-zero $\Delta^{33}S$ values during the transfer of both oxidized and reduced sulfur species to the surface (Pavlov and Kasting, 2002) and for the maintenance of the $\Delta^{33}S$ differences between oxidized and reduced species in sedimentary environments (Farquhar et al., 2000).

The oxidized species, in the form of sulfate, will reside predominantly in the oceans and will impart the negative $\Delta^{33}S$ signature on the Archean ocean sulfate reservoir (Farquhar et al, 2001). The reduced sulfur species, S_8 aerosols, are relatively insoluble, and will collect on the seafloor, and likely be reduced, biotically or abiotically, to form sedimentary pyrite. The end result of this process is a number

of Archean sulfur reservoirs with distinct $\Delta^{33}S$ compositions that can be used as a chemically-conservative tracer of sulfur transfer through Archean geological environments (Farquhar et al., 2002; Farquhar and Wing, 2003).

1.4 Applications for Terrestrial Systems

Stable isotope ratios, recorded in the rock record, have been used extensively in investigations of paleoenvironments, and the evolution of terrestrial, geological and biological processes. Interpretations of the isotopic record are limited by the fact that different physical processes can produce identical isotope ratios. The mass-independent fractionation record of sulfur in the Archean is not subject to this limitation, because there is only one known mechanism for producing such fractionations (photolysis in the Archean atmosphere, and transfer to surface), and because once a $\Delta^{33}S$ signature has been imparted on a surface sulfur species, it can only be altered by mixing with a sulfur reservoir with a different $\Delta^{33}S$ composition. This property is that of a conservative tracer. The conservative nature of $\Delta^{33}S$ allows it to be used to trace interactions between surface sulfur reservoirs with different $\Delta^{33}S$ values.

Oxidized and reduced sulfur species transferred to the surface have characteristic signatures: volcanic (juvenile) sulfur has $\Delta^{33}S$ value = 0‰; Archean oceanic sulfate is proposed to have a negative $\Delta^{33}S$; and reduced sulfur is thought to have, generally, a positive $\Delta^{33}S$ value (Ono et al., 2003; Farquhar and Wing, 2003).

The utility of $\Delta^{33}S$ signatures as a tracer of surface processes has not yet been fully explored. Archean seafloor hydrothermal systems provide a natural laboratory

to study the movement of sulfur between the surface reservoirs, due to the possibility of sulfur from the oceans, sediments, and volcanic sources being incorporated into this single system. Seafloor hydrothermal systems are well-documented because of their link to the genesis of VMS deposits (Ohmoto, 1996). Long standing questions related to the formation of VMS deposits are the source(s) of sulfur and the origin and evolution of the ore-forming fluid (Huston et al., 2001). There has been much debate over whether the primary source of sulfur in Archean VMS deposits is reduced sulfur, leached from the oceanic crust, or direct input of magmatic sulfur. Seawater sulfate is considered a major source of sulfur for Phanerozoic VMS deposits (Sangster, 1968). The importance of seawater sulfate in the formation of Archean deposits is not clear, because of the uncertainty of sulfate concentrations in the Archean ocean (Vearncombe et al., 1995; Strauss, 2003). Some workers suggest the Archean ocean may have been sulfate-rich (>10mM) since the early Archean, and a significant component of sulfur in Archean hydrothermal systems may have been seawater sulfate (Ohmoto, 1992). This model implies an oxygen-rich atmosphere as early as 3.5 Ga, which resulted in oxidative weathering of continents and a source of sulfate to the oceans. This also may have resulted in bacterial reduction of oceanic sulfate in the early Archean (Ohmoto et al., 1992). Alternately, anoxygenic photosynthesis in an oxygen-poor environment may have resulted in low (<1mM) ocean sulfate concentrations, and the onset of bacterial sulfate reduction did not occur until 2.7 - 2.5 Ga (Canfield and Raiswell, 1999). The concentration of sulfate in the Archean ocean is further constrained by Habicht et al (2002), who propose concentrations of <200μM, based on comparisons of fractionation of sulfur by bacterial sulfate

reduction at different concentrations of sulfate, and measured $\delta^{34}S$ values in the rock record. The model of Farquhar and Wing (2003) also suggests low atmospheric oxygen values. However, the source of sulfate in the oceans in this model is aerosol deposition of photochemically-derived sulfate from the atmosphere. Estimates of the concentration of oceanic sulfate in a system, where the only source of sulfate is the atmosphere, are < 1mM (Walker and Brimblecombe, 1982).

Dissimilar $\Delta^{33}S$ values for the volcanic sulfur, seawater sulfate and sedimentary sulfide make mass-independent fractionation signatures an ideal tool for tracing the potential incorporation of seawater sulfate, and other sulfur sources in hydrothermal systems. Ultimately, this tool may provide insights into the nature of Archean hydrothermal systems and the formation processes of Archean VMS deposits.

1.5 Ore-forming Processes in Volcanogenic Massive Sulfide (VMS) Deposits

Volcanogenic massive sulfide (VMS) deposits are accumulations of sulfide minerals that form below or at the seafloor by the action of hydrothermal circulation (Franklin et al., 1981). They are found in many different geological environments, both modern and ancient, but are invariably associated with submarine extrusive volcanic activity (Ohmoto and Skinner, 1983). VMS deposits are often classified on the basis of their host-rock composition, with the focus on relative amounts of felsic, mafic, and ultramafic volcanics, and sedimentary rocks (Barrie and Hannington, 1999). Understanding of the processes which lead to the formation of VMS deposits was greatly enhanced in the last three decades with the discovery of active

hydrothermal vents on the seafloor (Edmond et al., 1979), allowing for the direct observation of ore formation (Ohmoto, 1996).

Volcanogenic massive sulfide deposits occur as stratiform orebodies within predominantly volcanic rocks, although, in some cases, the ore is hosted by local sedimentary rocks, within volcanic strata (Franklin et al., 1981). The mineralogy of VMS deposits is dominated by variable amounts of Cu, Zn and Pb-rich sulfides. Internal metal zoning within the orebodies, caused by different temperatures of precipitation for the metal sulfides, results in a Cu/Cu+Zn+Pb ratio that increases with depth. A Cu-rich stockwork feeder zone, in intensely altered rocks, often underlies the orebodies (Franklin et al., 1981). Submarine exhalative features may be present as well, indicating direct venting of metal sulfides into the water column from beneath the seafloor (Ohmoto, 1996).

The sources of both metals and sulfur are linked to hydrothermal circulation through oceanic crust (Franklin et al, 1981). Cold seawater seeps into the crust where it is heated by shallow igneous bodies (Fig. 4) (Gibson et al., 1999). At low initial temperatures (<150ºC), fixation of alkalis such as Na and K in the crust occurs, and Mg from seawater is precipitated as smectite (Alt, 1999). Once fluid temperatures increase, much of the dissolved seawater sulfate precipitates as anhydrite, and remaining Mg reacts with water to form chlorite, causing the pH of the fluid to decrease (Alt, 1999). Any remaining sulfate is inorganically reduced, either by oxidation of reduced Fe in the host rock (Huston et al., 2001):

$$HSO_4^- = 8FeO_{Rock} + H^+ = H_2S + 4Fe_2O_3 \quad (1.5)$$

or by oxidation of pyrrhotite to pyrite (Shanks and Seyfried, 1987):

$$8FeS + 10H^+ + SO_4^{2-} = 4FeS_2 + H_2S + 4H_2O + 4Fe^{2+} \quad (1.6).$$

As temperatures reach a maximum (>350ºC) at the reaction zone, metals and reduced sulfur are leached from the rock (Fig. 4) (Alt, 1999). Possible direct contributions of metal and sulfur from magmatic fluids have also been suggested (Yang and Scott; 1996). The fluid ascends rapidly to the surface where it mixes with seawater, and precipitation of sulfide minerals occurs (Franklin et al., 1981), resulting in subsurface mineralization or seafloor venting at black smokers (Alt, 1999).

Changes in environmental conditions over time, such as ocean sulfate concentrations, global thermal regimes, and biological evolution, may have resulted in formation processes for modern VMS deposits that differ from that of ancient examples.

1.6 Accomplishments of this Thesis

The purpose of this thesis is to investigate the application of mass-independent ($\Delta^{33}S$) sulfur signatures as a tracer for sulfur mobility in Archean hydrothermal systems. In particular, the following primary questions have been addressed:

1. Can $\Delta^{33}S$ values be used to trace different sources of sulfur through ancient hydrothermal systems?
2. What are the sources of sulfur for Archean VMS deposits?

In attempting to answer these primary questions, other questions related to Archean surface environment, such as the chemistry of the Archean oceans, processes occurring at seafloor hydrothermal vent sites and the possibility of $\Delta^{33}S$ values as an exploration vector for ore deposits were investigated.

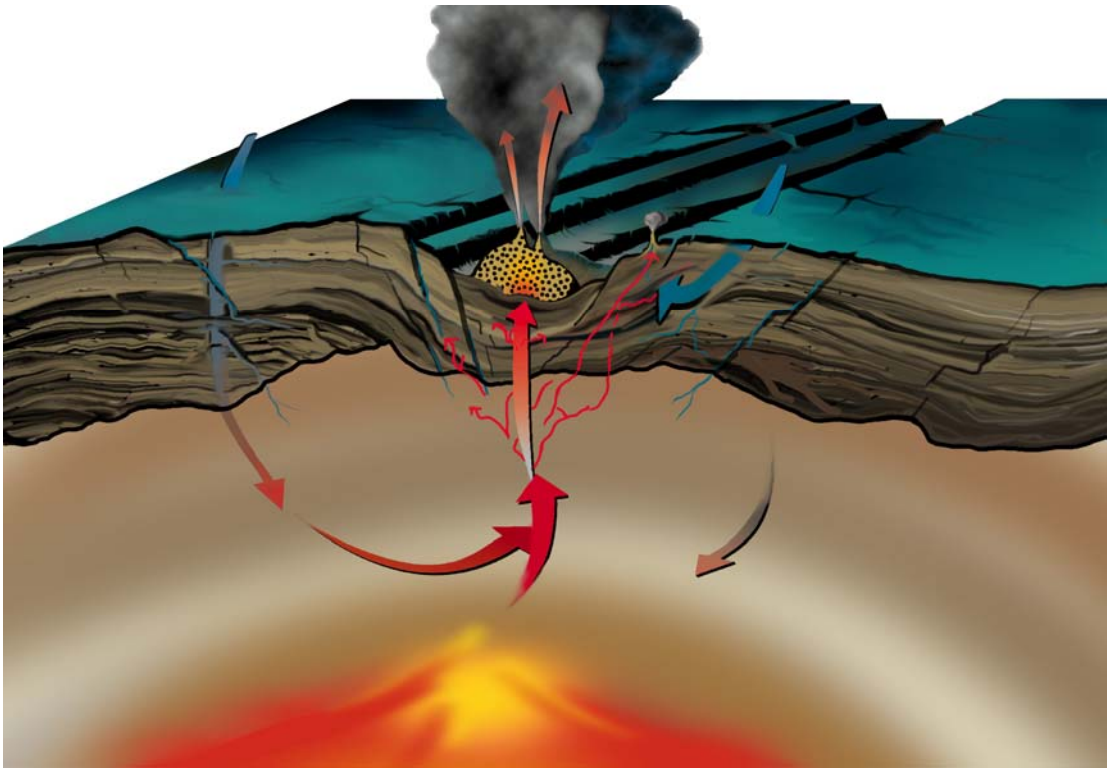

Figure 4: Cross-section of a seafloor hydrothermal system. Cold water infiltrates the crust and is heated by shallow igneous activity. Metals are leached from the rock at high temperatures. The fluid migrates to the surface along normal faults, and mixture of hot hydrothermal fluid with cold seawater causes precipitation of sulfide minerals at and/or below the seafloor surface. Venting of metal-rich fluid at the surface produces black smokers. Illustration by E. Paul Oberlander, Woods Hole Oceanographic Institution. Used with permission.

The use of $\Delta^{33}S$ values to evaluate isotopic equilibrium in sulfide mineral pairs is a new application of multiple sulfur isotopes that can be directly applied to Archean ore deposit studies. This new tool for equilibrium evaluation will allow for more reliable sulfur-isotope paleothermometry studies and differentiation of ore forming events in single ore deposits.

Finally, this study will potentially lead to further applications of multiple sulfur isotopes as a geochemical tool for investigations for Archean surface processes.

Sulfur isotope measurements of a full suite of samples from a well characterized Archean VMS deposit were necessary for the scope of this study. The 2.7 Ga Kidd Creek deposit, in Ontario, Canada, is a world-class VMS deposit, and has been the focus of many studies (most notably a major detailed study in the 1990s by industry, government and university researchers, which resulted in the publication of an *Economic Geology Monograph*) (Hannington and Barrie, 1999). This study has led to a better understanding of the tectonic and surface environment in which the deposit formed, as well as the physical and chemical processes involved in its formation. The extensive geological and geochemical data available from this deposit makes it an ideal location for this detailed investigation of the distribution of $\Delta^{33}S$ signatures in an ancient seafloor hydrothermal setting.

Chapter 2: Geological Background and Previous Work

2.1 The Kidd Creek Volcanogenic Massive Sulfide Deposit

The Kidd Creek VMS deposit is situated in the Abitibi granite-greenstone belt, within the Superior craton, in eastern Ontario, Canada. The Abitibi subprovince is thought to represent a series of granite-greenstone terrains, formed by accretion of volcanic arcs and oceanic plateaus from ~2.8 to ~2.6 Ga (Langford and Morin, 1976; Jackson and Cruden, 1995; Ludden and Hubert, 1986). The ore deposit is located in a suite of bimodal (felsic, mafic and ultramafic) volcanics of the Kidd-Munro assemblage, which formed between 2717 and 2711 Ma (Corfu, 1993; Bleeker, 1999). The mine succession consists of basal komatiitic flows, followed by a lower massive rhyolite unit and an upper fragmental rhyolite unit, which hosts the sulfide ore (Barrie, 1999; Prior et al., 1999). Above the rhyolite is a quartz porphyry rhyolite, followed by mafic volcanic rocks consisting of pillow lavas and breccias, with interflow graphitic argillites (Hannington et al., 1999). The entire mine sequence is intruded by gabbroic dykes and a large gabbroic sill overlies the quartz porphyry. The lower boundary of the mine sequence is a fault or unconformity that separates the volcanic succession from greywackes of the Porcupine Group that are younger than 2699 Ma (Bleeker and Parrish, 1996).

The mine stratigraphy at Kidd Creek has undergone multiple deformation events, producing ore bodies that may be truncated, stretched, and over-thickened (Bleeker, 1999). A series of folding events have produced a large scale interference

structure (Hannington et al., 1999). The deformation is systematic throughout the mine stratigraphy, which has made it possible to reconstruct the original geometry, and the depositional history of the ore deposit (Bleeker, 1999).

The volcanic succession at Kidd Creek was erupted during seafloor rifting, likely in a back-arc basin (Bleeker et al., 1999) or mid-oceanic rift (Prior et al., 1999). Hydrothermal circulation of seawater, driven by shallow igneous activity at the spreading center, caused focused discharge of an evolved fluid along steeply dipping normal faults, which bound a topographic low on the seafloor (Huston and Taylor, 1999). Precipitation of sulfide minerals occurred when the hot fluid mixed with cold seawater (Pottorf and Barnes, 1983). At Kidd Creek, ore precipitation occurred mostly below the seafloor, by infilling and replacement of rhyolite flows and volcanoclastics in a seafloor graben or half-graben (Hannington et al., 1999a). Minor focused venting of hydrothermal fluids at the seafloor resulted in surface mineralization and the development of vent complexes (Hannington et al., 1999a).

Massive sulfide occurs as three distinct lenses within the rhyolite: the north, central, and south orebody (Fig. 5) (Hannington et al., 1999a). The lenses are composed primarily of massive pyrite and sphalerite, with minor pyrrhotite and galena (Fig. 6A). Evidence of seafloor exposure and vent complexes takes the form of sinters and sulfide debris flows near the top of the north orebody, and suggests that parts of this lens were exposed at the surface (Hannington et al., 1999a). The lack of such features in the central and south orebodies suggests that these lenses formed entirely below the seafloor.

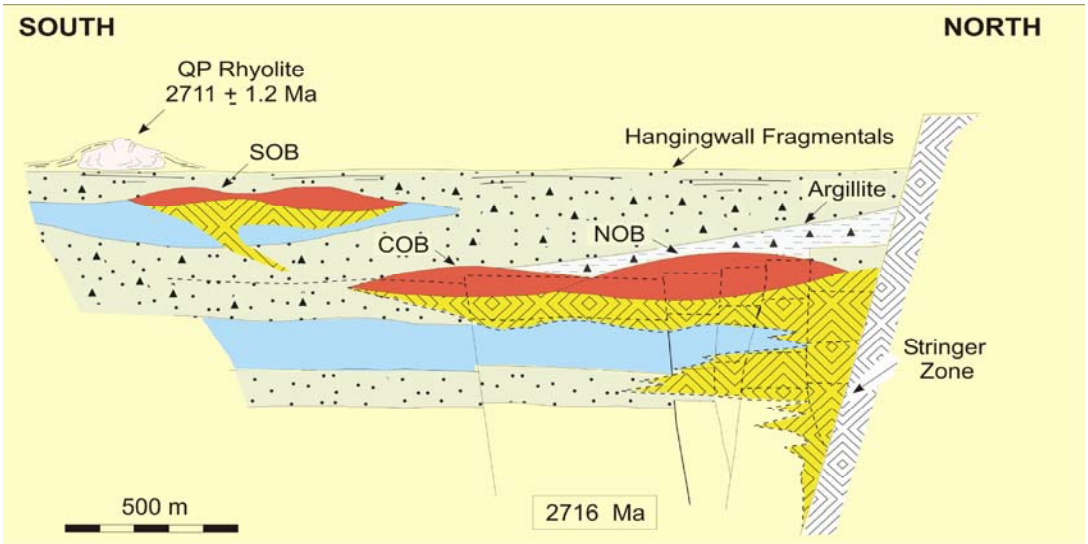

Figure 5: Cross-section (reconstructed) of Kidd Creek, showing the massive sulfide lenses (red), with underlying Cu-rich feeder zones (yellow) in a rhyolite host rock. The faulted is bounded to the north by a major structural discontinuity. (NOB = North Ore Body; COB = Central Ore Body; SOB = South Ore Body). Modified from Hannington et al. (1999)

The underside of each lens has a characteristic Cu-rich zone, composed primarily of chalcopyrite, which formed by replacement of sphalerite during a late stage injections of Cu-rich fluids (Fig. 6C) (Hannington et al., 1999). The sphalerite reprecipitated at higher levels in the massive sulfide lenses. Beneath the south orebody is a high-grade bornite zone, which represents an influx of a large amount of an end-member, Cu-rich fluid, during the late stages of ore formation Fig. 6D) (Hannington et al., 1999b). An extensive Cu-rich stockwork feeder zone underlies the ore lenses, and reflects the upward-directed, down-temperature flow pathway of the metal-rich hydrothermal fluid (Fig. 5) (Koopman et al., 1999). For the purposes of this discussion, the ore lenses, bornite zone and Cu-rich stringer zones are collectively referred to as massive sulfide.

Sulfides (mostly sphalerite and pyrite) also occur along the flanks of the orebodies, as minor stringers and disseminations (Hannington et al., 1999a). These zones of stratabound stringer and disseminated mineralization, hosted in brecciated rhyolite, extend laterally from the massive sulfide lenses (Fig. 6B). The concentration of sulfide minerals in these zones is significantly less than the concentrations in the massive sulfides, and the ore minerals are referred to as wall-rock sulfides.

Stratigraphically above the north and central orebodies, but in the footwall of the south orebody, is a graphitic argillite that is rich in sulfide debris flows, as well as pyrite nodules (Fig. 6F). These sulfides are thought to have a hydrothermal or diagenetic origin (Hannington et al., 1999). This sedimentary unit likely formed during a hiatus in volcanic activity on the seafloor. Debris flows, composed of pyrite

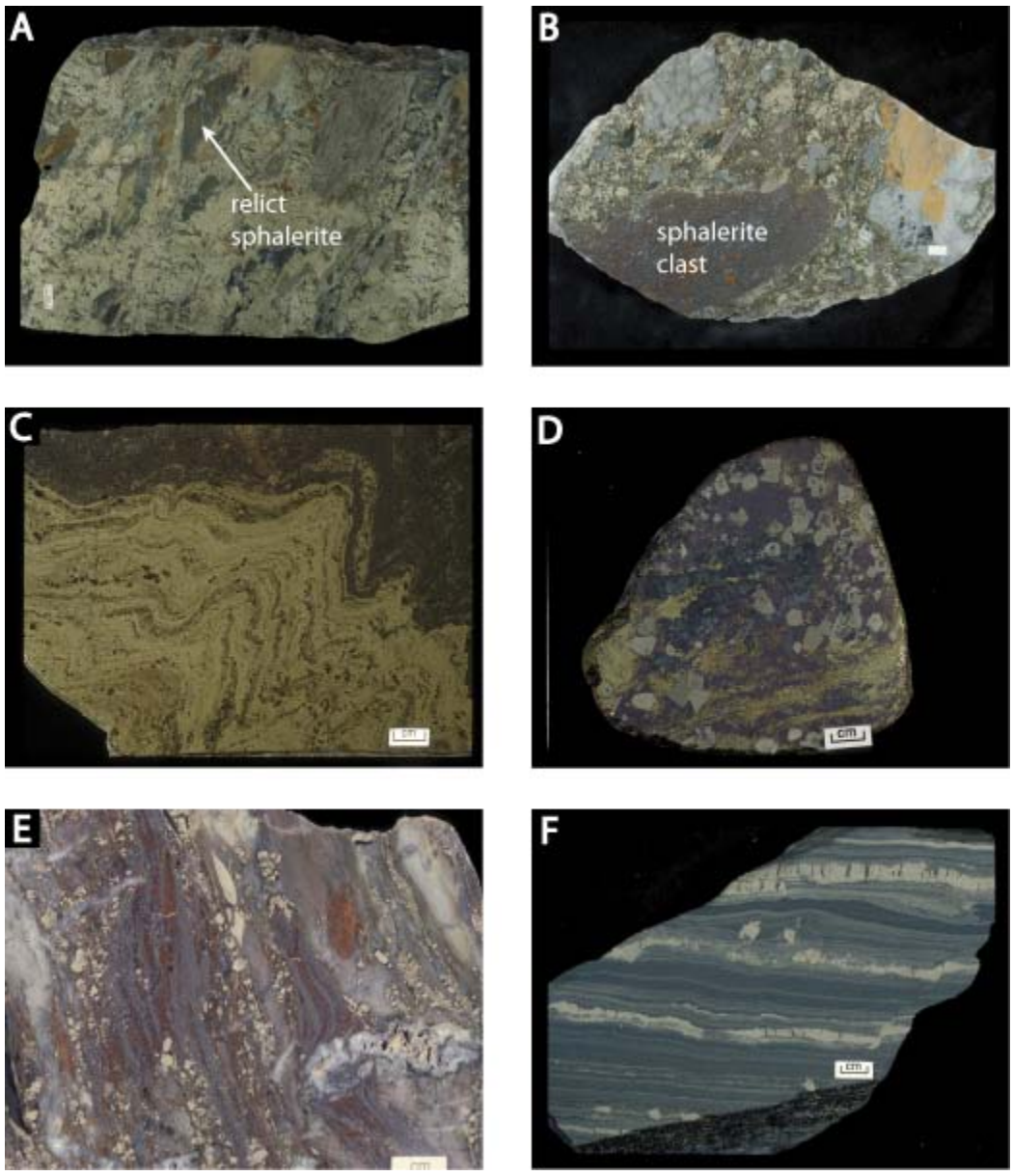

Figure 6: Representative ore textures from Kidd Creek. A. Fragmental massive pyrite and relict sphalerite clasts from top of massive sulfide lens. B. Pyrite and galena rich fragmental rhyolite, with a large sphalerite clast. C. Folded contact between massive sphalerite and chalcopyrite at base of north orebody. D. Massive bornite with relict chalcopyrite and pyrite porphyroblasts. E. Laminated quartz and sphalerite sinter above north orebody. F. Laminated graphitic argillite with graded sphalerite-rich turbidites. Photographs courtesy of Mark Hannington, University of Ottawa.

and sphalerite, occur within the argillite. These sulfide flows contain graded bedding, and other sedimentary features, such as load casts and flame structures. These turbiditic flows are thought to represent chimney collapse and mass-wasting events of vent sulfides from the topographically high hydrothermal mound at the discharge site, into the graben basin (Hannington et al, 1999a). Sulfides from these flows are referred to as sulfide turbidites.

Direct precipitation of sulfide minerals onto the seafloor on the north orebody resulted in sulfide-rich chemical sedimentary crusts (Fig 6E). These crusts are found predominantly at the top of the north orebody, which was exposed at the seafloor. Samples from these chemical crusts are referred to as sulfide-rich sinter.

2.2 Previous Sulfur-isotope Studies of Kidd Creek

The sulfur isotope ratios of Kidd Creek sulfides have been investigated in two previous studies (Strauss, 1989; Hannington et al., 1999a). In both studies, sulfur isotopes were measured from sulfides in the main orebodies, and hydrothermal sulfides in the argillitic sediments above the orebodies.

The $\delta^{34}S$ values from the main massive sulfide bodies clustered near 0‰, which is typical for Archean massive sulfide deposits (Franklin et al., 1981). Strauss (1989) interprets this isotopic signature to indicate a magmatic source for the sulfur in the massive sulfides. The non-ore sulfides within the argillites have slightly more positive $\delta^{34}S$ values. Strauss (1989) interprets these values to result from inorganic reduction of seawater sulfate. Bacterial sulfate reduction is not considered a mechanism in the formation of these argillite-hosted sulfides, insofar as biogenic

sulfides precipitated by sulfate-reducing bacteria are not believed to appear before 2.4 to 2.2 Ga (Strauss, 1989).

Hannington et al. (1999a) observed little variation in $\delta^{34}S$ values between the three main ore lenses, and suggest a homogenous sulfur source for the orebodies. The isotopic compositions of the massive sulfides are thought to reflect the primary hydrothermal signature. The sulfides within the argillite are isotopically heavier than the massive sulfides, and have a larger range in $\delta^{34}S$ values. This is interpreted to reflect variable sulfur sources within these units, which may have included inorganic reduction of seawater sulfate.

Chapter 3: Methods

3.1 Sulfur Isotope Measurements

Sulfide mineral samples from the Kidd Creek VMS deposit were collected by Mark Hannington as part of a comprehensive study of the ore deposit that resulted in the publication of *Economic Geology Monograph 10*. Samples were collected from the open pit, underground mining operations, diamond drill core, and surrounding surface exposures. Regional hydrothermal sulfides from the Kidd-Munro assemblage were also included. The samples were crushed and minerals separated at the Geological Survey of Canada. Sulfur isotope measurements on sulfide mineral separates were performed at the Stable Isotope Laboratory, University of Maryland.

Sulfur isotope analyses largely followed the methods of Rumble et al. (1993) and Hu et al. (2003). Sulfides were converted to SF_6 gas and other fluoride compounds by heating the minerals under a ~40 Torr F_2 atmosphere with a 25W CO_2 infrared laser (λ = 10.6 μm). The resulting SF_6 and condensable impurities were condensed and separated from non-condensable gaseous fluoride compounds using an N_2 cryogenic trap (-196˚C). The liquid nitrogen trap was then evacuated of non-condensable gases and warmed with an ethanol slush (-110˚C) to release SF_6. The SF_6 was transferred to an injection loop and then passed through a gas chromatograph to separate and remove remaining impurities. Purified SF_6 was introduced to a ThermoFinnigan MAT 253 dual-inlet gas-source mass spectrometer, which analyses gaseous compounds by first ionizing the compounds to SF_5^+, then accelerating them

through a flight tube where their paths are deflected by a magnetic field. The amount of deflection is a function of the charge-to-mass ratio of the compounds. The sulfur isotope abundances for this project were measured by monitoring the $^{32}SF_5^+$, $^{33}SF_5^+$, $^{34}SF_5^+$ ion beams at m/z = 127, 128, and 129, respectively. We did not carry out the multiple purifications through the gas chromatograph that are required to remove compounds producing isobaric interferences at m/z = 131 (such as C_3F_5) (Gao and Thiemens, 1991; Rumble et al., 1993; Hu et al., 2003). Therefore, although the $^{36}SF_5^+$ ion beam was monitored and ^{36}S measurements are included in the results, only ^{32}S, ^{33}S, and ^{34}S measurements are used for purposes of our geologic interpretation and discussion.

3.2 Interpretational Framework

Traditional three-isotope plots ($\delta^{33}S$ vs. $\delta^{34}S$) are the most common way to express multiple isotope ratios. These plots clearly illustrate the mass-dependent fractionation relationship between the isotope ratios, and samples that do not strictly follow this relationship (Fig. 1). However, for typical natural ranges in $\delta^{34}S$ (and, by association, $\delta^{33}S$) values, $\Delta^{33}S$ values must be large to be clearly identified. In other words, data points that have only small, but statistically significant (resolvable within uncertainty) $\Delta^{33}S$ values will plot close to the terrestrial fractionation line, and thus may be wrongly interpreted as having a mass-dependent isotopic composition. Samples with $\Delta^{33}S$ values between -0.01 and 0.01‰ are considered mass-dependent.

Results of isotopic analyses of individual sulfide samples can also be plotted on a $\Delta^{33}S$ vs. $\delta^{34}S$ diagram. The two axes can be scaled independently so that the maximum range in $\Delta^{33}S$ as well as $\delta^{34}S$ values can be displayed. Samples with mass-

dependent sulfur will have a $\Delta^{33}S$ value near 0 per mil. The $\Delta^{33}S$ of samples with an added component having negative $\Delta^{33}S$ values, such as Archean sulfate, will reflect this contribution and will plot below the x-axis. Samples that have incorporated sulfur with positive $\Delta^{33}S$, such as Archean reduced sulfur in sediments, will plot above the x-axis. Data arrays on this type of plot can also be interpreted for sample sets that exhibit either small or large ranges in $\delta^{34}S$ and $\Delta^{33}S$ values.

Paleotemperatures were calculated from sulfide mineral pairs. The pairs consisted of combinations of six different sulfide minerals, and eight independent pairs were analyzed. Calibrations for isotope thermometers are from Ohmoto and Rye (1979) and are shown in Table 1.

3.3 Analytical Uncertainties

Reproducibility of the entire measurement procedure was evaluated by repeat analyses of an in-house pyrite working standard (see Appendix). Multiple measurements of this standard (n=10) indicate that $\delta^{34}S$ was measured with an external reproducibility of ±0.22 ‰ (1σ), and $\delta^{33}S$ with a long-term reproducibility of ±0.11 ‰ (1σ). Similar tests for $\Delta^{33}S$ yield an external reproducibility of ±0.009 ‰ (1σ). Most of the variation in $\delta^{33}S$ and $\delta^{34}S$ is due to minor mass-dependent fractionation inherent in the measurement procedure, as indicated by the difference between the experimentally determined reproducibility for $\Delta^{33}S$ (0.009 ‰) and the uncertainty predicted by propagation of uncorrelated experimental uncertainties for $\delta^{33}S$ and $\delta^{34}S$ through the definition of $\Delta^{33}S$ (0.158 ‰) (see Apendix).

Table 1: (from Ohmoto and Rye, 1979)

$$T = \sqrt{\frac{A \times 10^6}{1000 \ln\left(\frac{\delta^{34}S_X + 1000}{\delta^{34}S_Y + 1000}\right)}}$$

Calibrations for Sulfur Isotope Thermometers

Mineral X	Mineral Y	Value "A"
Pyrite	Galena	1.03
Pyrite	Sphalerite or Pyrrhotite	0.3
Chalcopyrite	Bornite	0.2
Sphalerite or Pyrrhotite	Chalcopyrite	0.15

Calculated $\Delta^{33}S$ values vary depending on the value of λ used in equation 1.3. Theorietical calculations indicate that equilibrium processes produce λ values that range from 0.513 to 0.518 (Hulston and Thode, 1965). This variation results in a $\Delta^{33}S$ value that can vary by 0.003 ‰, for every per mil shift in a $\delta^{34}S$ value. The range in measured $\delta^{34}S$ values at Kidd Creek results in a possible variation in $\Delta^{33}S$ values of 0.01 ‰, which is less than the 2σ experimental reproducibility of the measured $\Delta^{33}S$ values (0.018 ‰).

Chapter 4: Results

4.1 Kidd Creek Sulfides

Sulfur isotope ratios ($\delta^{33}S$, $\delta^{34}S$, and $\Delta^{33}S$) of fifty-five sulfide samples from the Kidd Creek ore deposit are presented in Table 2. The results are illustrated on a traditional three-isotope plot (Fig. 7) and on a $\Delta^{33}S$ vs. $\delta^{34}S$ plot (Fig. 8). Because of the expanded scale, the $\Delta^{33}S$- $\delta^{34}S$ diagram in Figure 8 illustrates more clearly the degree of non-mass-dependence in the samples. The data include sulfides from the main ore deposit as well as sulfides from the surrounding country rock. The $\delta^{34}S$ values range from -4.26 to 5.46 ‰, with a mean value of 0.72 (± 1.82) ‰ (1σ). Mass-independent signatures ($\Delta^{33}S$) were calculated for all samples, using equation (1.3). Values of $\Delta^{33}S$ range from -1.50 to 1.12 ‰.

The analyzed samples are divided into four groups, based on textural features of the sulfides and the host rock. Together, these features ultimately correlate to the location and environment of precipitation within the ore deposit. The most common ore type is massive sulfide, which occupies the three main ore lenses near the top of the deposit succession, and their accompanying Cu-rich feeder zones. Also included is the high-grade bornite zone beneath the south ore body. The massive sulfides represent precipitation of ore by epigenetic replacement of rhyolite below the seafloor during mixing of the hot hydrothermal fluids with cold seawater. Sulfide minerals analyzed in this study include pyrite, sphalerite, chalcopyrite, pyrrhotite, galena and

Table 2: Isotopic analyses of sulfides from Kidd Creek

Sample	Mineral	$\delta^{33}S_{V\text{-}CDT}$ (‰)	$\delta^{34}S_{V\text{-}CDT}$ (‰)	$\delta^{36}S_{V\text{-}CDT}$ (‰)	$\Delta^{33}S$ (‰)	$\Delta^{36}S$ (‰)
Massive Sulfides						
KCP53_2	Gn	-1.64	-3.01	-5.03	-0.09	0.68
KC5	Bn	-0.84	-1.57	-1.93	-0.03	1.05
KC350_A1	Bn	-0.81	-1.51	-2.33	-0.03	0.54
KC349	Bn	-0.41	-0.73	-0.71	-0.04	0.67
KC350_A2	Cp	-0.40	-0.71	-0.74	-0.04	0.61
KC5	Cp	-0.39	-0.71	-0.64	-0.03	0.70
KC8	Py	-0.28	-0.53	9.46	-0.01	10.47
KC17B	Sp	-0.31	-0.43	-0.07	-0.09	0.75
KC93	Sp	-0.19	-0.31	1.62	-0.03	2.21
MH184_1	Cp	-0.18	-0.31	0.43	-0.02	1.02
KC451_1	Po-Sp	-0.20	-0.28	0.05	-0.05	0.58
KC48	Py	-0.19	-0.27	0.22	-0.05	0.73
KC29B	Sp	-0.18	-0.26	0.46	-0.05	0.95
KC29B	Sp	0.02	0.12	0.96	-0.04	0.74
KC86	Sp	-0.13	-0.10	0.55	-0.08	0.74
KC36	Cp	-0.06	-0.06	0.62	-0.03	0.73
KC36	Cp	0.42	0.83	2.12	-0.00	0.55
KC451_2	Sp	-0.06	-0.04	0.63	-0.04	0.71
KCP36B	Cp	-0.03	-0.01	0.71	-0.03	0.74
KC12	Cp	0.01	0.08	0.54	-0.04	0.39
KC12	Cp	-0.03	-0.03	0.46	-0.02	0.51
KC93	Po	0.03	0.16	0.97	-0.05	0.66
KC6B	Cp	0.05	0.17	0.95	-0.04	0.62
KC96	Cp	0.06	0.18	0.76	-0.03	0.42
KC83A	Py	0.12	0.24	1.11	-0.01	0.67
KC43	Cp	0.09	0.28	8.32	-0.05	7.80
KC111	Sp	0.12	0.34	1.03	-0.05	0.39
KC43	Po	0.14	0.37	1.16	-0.05	0.45
KC9A	Cp	0.20	0.37	1.52	0.01	0.81
KC44	Cp	0.25	0.47	1.71	0.01	0.83
KC83A	Sp	0.20	0.51	1.52	-0.07	0.55
KC121	Py	0.24	0.55	1.71	-0.04	0.67
KC121	Py	0.21	0.50	1.66	-0.04	0.72
KC65A	Cp	0.35	0.73	1.48	-0.02	0.09
KC29B	Po	0.37	0.73	1.90	0.00	0.50
KC15	Py	0.27	0.76	2.42	-0.12	0.97
KC110	Sp	0.58	1.15	3.06	-0.01	0.86
KC53-1	Py	0.63	1.34	2.95	-0.06	0.40
KC52B	Py	0.73	1.79	3.71	-0.19	0.30
KC95	Cp	1.15	2.22	4.69	0.00	0.47

(Continued next page)

Table 2: Isotopic analyses of sulfides from Kidd Creek (cont.)

Sample	Mineral	$\delta^{33}S_{V\text{-}CDT}$	$\delta^{34}S_{V\text{-}CDT}$	$\delta^{36}S_{V\text{-}CDT}$	$\Delta^{33}S$	$\Delta^{36}S$
Wallrock Sulfides						
KC307	Py	0.32	0.69	1.54	-0.04	0.22
KC475	Py	1.36	2.78	6.14	-0.07	0.85
KC375	Py	2.34	4.84	10.02	-0.15	0.80
Sulfide-rich Sinter						
KCP47	Py	-0.16	-0.15	0.19	-0.08	0.48
KCP45A	Py	0.52	0.18	0.65	0.43	0.31
KC130	Py	1.73	1.72	3.17	0.84	-0.09
Sulfide Turbidites						
KCC13-2	Py	-1.49	-4.26	-8.99	0.71	-0.92
KCR34-1	Py	-2.04	-3.18	-5.87	-0.40	0.16
KCC13-1	Py	-0.38	1.14	3.58	-0.96	1.41
KC129	Py	0.59	1.33	3.39	-0.09	0.85
KCC14-3	Py	1.81	1.47	2.47	1.05	-0.32
KCC14-1	Py	0.75	1.57	3.63	-0.06	0.65
KCR45B	Py	0.41	1.66	3.86	-0.44	0.71
KCR34-2	Py	0.56	1.91	4.62	-0.43	0.98
KCP5	Py	0.90	1.99	4.55	-0.13	0.76
KCP5	Py	0.95	2.08	4.49	-0.12	0.55
KCC14-2	Py	1.10	2.01	4.17	0.06	0.35
KCR44	Py	2.75	3.18	4.64	1.12	-1.40
KCR44	Py	2.79	3.27	4.79	1.11	-1.43
KCCARN-4	Py	1.23	4.92	11.03	-1.31	1.66
KC4509	Py	1.31	5.46	12.15	-1.50	1.75
KC4509	Py	1.34	5.20	11.80	-1.34	1.90

Note: Samples with repeat measurements are plotted in Figures 7 and 8 as average values.

Table 3: Mineral Abbreviations (from Kretz, 1983):

Mineral	Abbreviation
Pyrite	Py
Pyrrhotite	Po
Sphalerite	Sp
Galena	Gn
Chalcopyrite	Ccp
Bornite	Bn

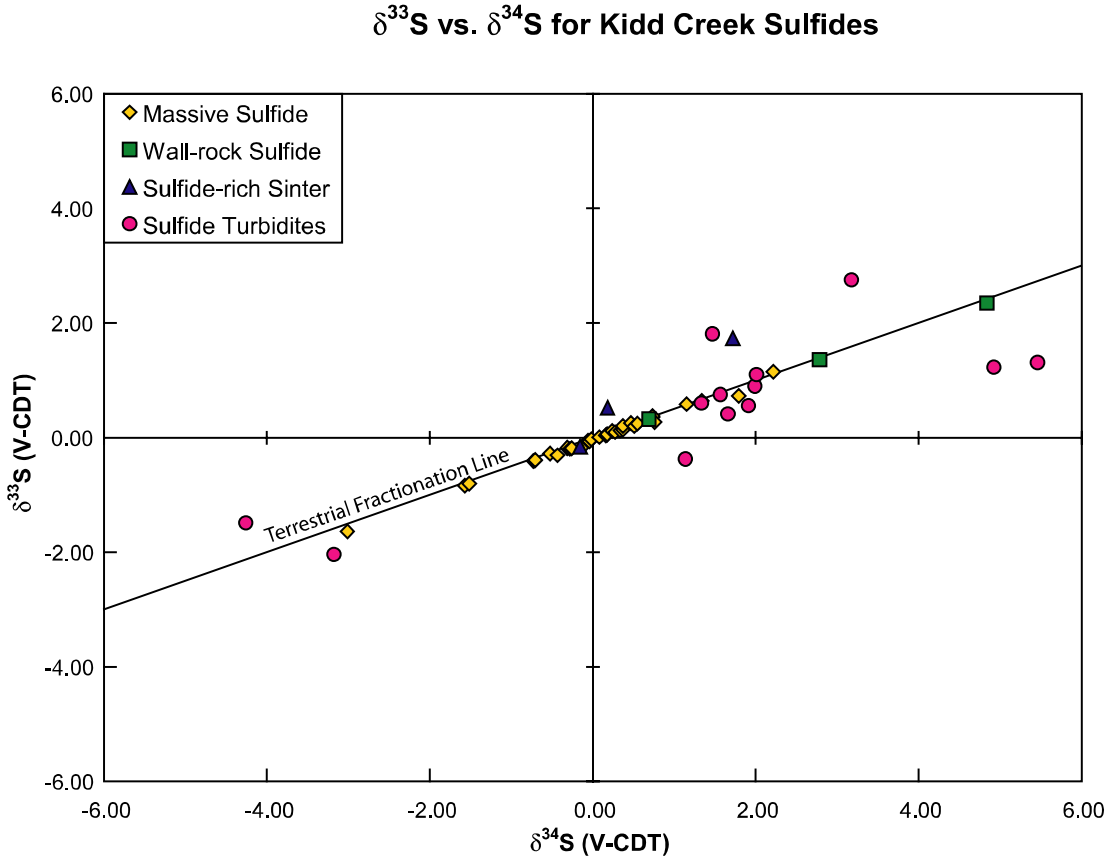

Figure 7: Traditional three-isotope plot of sulfides from Kidd Creek (similar to Figure1). Samples with mass-independent signatures plot above or below the TFL.

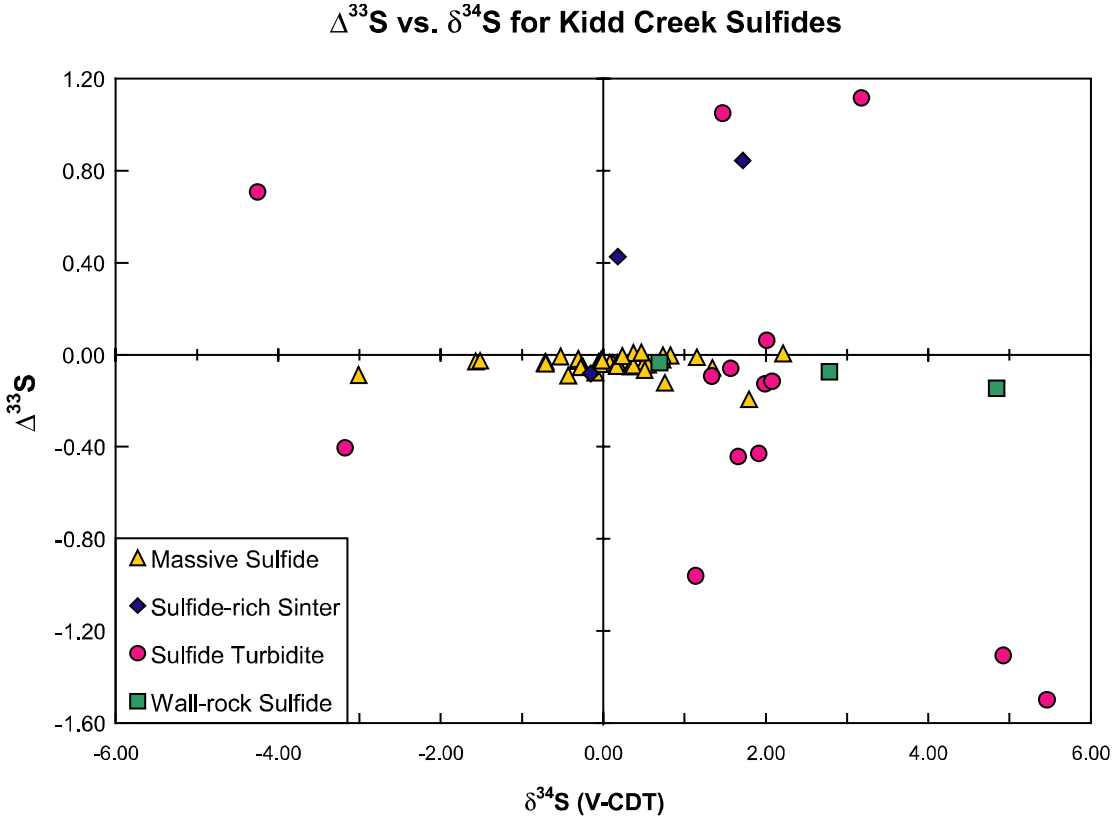

Figure 8: This plot shows in more detail the $\Delta^{33}S$ values of the sulfides at Kidd Creek. The massive sulfides and wall-rock sulfides have a narrow range of $\Delta^{33}S$ values, whereas the sulfide-rich sinter and sulfide turbidite show large variations in $\Delta^{33}S$ values.

bornite. The massive sulfides have a $\delta^{34}S$ range of -3.01 to 2.22 ‰ and a $\Delta^{33}S$ range of -0.19 to 0.01 ‰ (n=36), showing a spread in $\delta^{34}S$ values with little variation in $\Delta^{33}S$ values. Of these samples, only three have positive $\Delta^{33}S$ values. The majority of the samples have negative $\Delta^{33}S$ values that do not overlap the mass-dependent line (x-axis in Fig. 8).

Wall-rock sulfides consist of pyrite and sphalerite staining within the fragmental rhyolite that hosts the main lenses (Koopman et al., 1999). Staining consists of microscopic disseminations and diffuse patches in silicified cherty breccias and occurs in the hanging wall of the deposit and laterally from the main lenses and precipitated from diffuse flow of hydrothermal fluids (Koopman et al., 1999). The $\delta^{34}S$ values of the three wall-rock sulfides analyzed range from 0.69 to 4.84 ‰, and the $\Delta^{33}S$ are all negative, with values that range from -0.15 to -0.04 ‰. This range is similar to the $\Delta^{33}S$ range in the massive sulfides.

The three samples grouped as sulfide-rich sinter represent sulfides that formed as direct precipitates on the seafloor at the site of hydrothermal discharge. These samples occur as pyrite replacing sphalerite in laminated argillaceous units that were deposited on the flanks of the seafloor hydrothermal mound. Sulfide sinter is not common at Kidd Creek, as the majority of sulfides precipitated below the seafloor. The $\delta^{34}S$ values of the sulfide sinter range from -0.15 to 1.72 ‰ (two of the three samples have $\delta^{34}S$ values that, within uncertainty, are 0 ‰) and the $\Delta^{33}S$ values range from -0.08 to 0.84 ‰. The only sulfide sinter sample with a negative $\Delta^{33}S$ value plots in the same field as the massive sulfides. The other two sulfide sinter samples have significantly higher $\Delta^{33}S$ values.

The final group of sulfides, sulfide turbidites, is interpreted to represent remains of collapsed sulfide vent chimneys. Collapses of the fragile chimneys result in sulfide-rich debris, which flows off the flanks of the hydrothermal mounds, and into graphitic and argillaceous sediments (Hannington, pers. comm.). Sulfides occur as laminated pyrite horizons with nodular pyrite and sphalerite replacement features. This group contains the largest variations in isotope ratios, both for $\delta^{34}S$ values and $\Delta^{33}S$ values. For the 13 samples analyzed, $\delta^{34}S$ values range from -4.27 to 5.46 ‰ and $\Delta^{33}S$ values range from -1.50 to 1.12 ‰. These values represent the extreme positive and negative $\delta^{34}S$ and $\Delta^{33}S$ values for all the hydrothermal sulfides analyzed at Kidd Creek.

4.2 Sulfide Mineral Pairs

Measured $\delta^{33}S$, $\delta^{34}S$, and $\Delta^{33}S$ values for eight sulfide mineral pairs are reported in Table 4, which also shows calculated paleotemperatures. All eight pairs are from massive sulfides of the main ore lenses or the bornite zone. For this study, minerals from the same hand specimen and, in most cases, from the same part of a hand specimen (i.e., a discrete mineral association or zone) are considered pairs. Co-precipitation is not a requirement for two minerals to be considered pairs.

Five mineral pairs from the north orebody were analyzed; three sphalerite-pyrrhotite pairs (#s 4, 5 and 6), a sphalerite-pyrite pair (#7) and a galena-pyrite pair (#3) (Table 4). The two bornite-chalcopyrite mineral pairs (#s 1 and 2) are from the high-grade bornite zone beneath the south orebody and the chalcopyrite-pyrrhotite pair (#8) is from the Cu-rich stringer zone, beneath the orebodies.

TABLE 4. Summary of Sulfur Isotopic Data of Mineral Pairs from Kidd Creek

Pair	Sample	Mineralogy	$\delta^{33}S_{V\text{-}CDT}$ (‰)	$\delta^{34}S_{V\text{-}CDT}$ (‰)	$\Delta^{33}S$[1]	Temperature[2] (Celsius)	σ_T[3] (Celsius)
1	KC 5	Bn	-0.84	-1.57	-0.029	209	234
	KC 5	Ccp	-0.39	-0.71	-0.030		
2	KC 350-A1	Bn	-0.81	-1.51	-0.026	227	245
	KC 350-A2	Ccp	-0.40	-0.71	-0.039		
3	KCP 53-2	Gn	-1.64	-3.01	-0.088	213	35
	KCP 53-1	Py	0.63	1.34	-0.056		
4	KC 93	Sp	-0.19	-0.31	-0.028	N/A[4]	N/A
	KC 93	Po	0.03	0.16	-0.050		
5	KC 451-1	Po	-0.20	-0.28	-0.054	N/A[4]	N/A
	KC 451-2	Sp	-0.06	-0.04	-0.041		
6	KC 29B	Sp	-0.18	-0.26	-0.050	N/A[4]	N/A
	KC 29B	Po	0.37	0.73	-0.004		
7	KC 83A	Py	0.12	0.24	-0.005	Reversed[5]	N/A
	KC 83A	Sp	0.20	0.51	-0.067		
8	KC 43	Ccp	0.09	0.28	-0.049	1018	2300
	KC 43	Po	0.14	0.37	-0.048		

[1]Values of $\Delta^{33}S$ are calculated using the relationship $\Delta^{33}S = \delta^{33}S - \left[\left(\frac{\delta^{34}S}{1000}+1\right)^{\lambda_{RFL}} - 1\right] \times 1000$

[2]Temperatures are calculated using values and equation from Table 10-1 of Ohmoto and Rye (1979)
[3]Uncertainties in temperature are calculated using method of Farquhar et al. (1993):

$$\sigma_T = \sqrt{\left[\frac{1000 \times A_{A-B}}{4\left(\ln\frac{1000+\delta^{34}S_A}{1000+\delta^{34}S_B}\right)^3}\right] \times \left[\frac{\sigma^2_{\delta^{34}S_A}}{\left(1000+\delta^{34}S_A\right)^2} + \frac{\sigma^2_{\delta^{34}S_B}}{\left(1000+\delta^{34}S_B\right)^2} + \frac{\sigma^2_{A_{A-B}}\left(\ln\frac{1000+\delta^{34}S_A}{1000+\delta^{34}S_B}\right)^2}{A^2_{A-B}}\right]}$$

[4]Equilibrium fractionation between sphalerite and pyrrhotite is negligible, therefore temperatures cannot be calculated from these minerals
[5]Pyrite must be isotopically heavier than sphalerite for a temperature to be calculated using these minerals

Chapter 5: Discussion

5.1 Sources of Sulfur at Kidd Creek

Sulfide minerals at Kidd Creek have a range of $\Delta^{33}S$ values indicating multiple sources of sulfur within the overall deposit. Minerals with positive $\Delta^{33}S$ values contain sulfur with a component of S_8 in the water column that has been reduced. Samples with negative $\Delta^{33}S$ values have a component of sulfur from seawater sulfate.

The range in $\Delta^{33}S$ values of the massive sulfides is small, and suggests a common source of sulfur for the three ore lenses, the bornite zone and the Cu-rich feeder zone, beneath the orebodies. The range in $\delta^{34}S$ values within the massive sulfides can be attributed to equilibrium fractionation between different sulfide minerals (see section 5.2).

The wall-rock sulfides are interpreted to be of hydrothermal origin and have a $\Delta^{33}S$ signature that is within the range of $\Delta^{33}S$ values of the massive sulfides, suggesting that the disseminated and nodular sulfides in the host rhyolite precipitated from the same fluid that formed the massive sulfides with their associated stringer zones.

Of the three sulfide samples extracted from the sulfide-rich sinter, two have $\Delta^{33}S$ values suggesting a significant component of sulfide that is reduced directly from the water column, likely by a chemical process. Anaerobic reduction by non-

photosynthesizing bacteria is not thought to be active at this time (Canfield and Raiswell, 1999). The third sample has an isotopic composition that plots within the range of the massive sulfides, indicating the possibility of a common source. The range in $\Delta^{33}S$ values between the three sinter samples indicates that the source of sulfur for sulfides precipitating from the hydrothermal fluid on the seafloor at the site of discharge is itself heterogeneous, with differing proportions of sulfur from sedimentary sources, seawater sulfate and volcanic sulfur.

The range in $\Delta^{33}S$ values for the sulfide turbidites shows the largest heterogeneity from a single genetic environment within the ore deposit. The $\Delta^{33}S$ values indicate significant contributions from volcanic sources, seawater sulfate and native sulfur.

The sulfides, categorized by environment of precipitation or deposition, can be further grouped according to their $\Delta^{33}S$ values. The massive sulfides and wall-rock sulfides all precipitated below the seafloor, and have a small range in $\Delta^{33}S$. The sulfide-rich sinter and sulfide turbidites can be grouped together as surface hydrothermal sulfides, and are distinguished by the large range in $\Delta^{33}S$ values. The difference in magnitudes and range of $\Delta^{33}S$ values between the surface and subsurface sulfides indicates a distinct difference in the sulfur chemistry of ore formation.

The subsurface ore has a slight, but consistently negative $\Delta^{33}S$ signature, indicating a minor contribution of seawater sulfate to an ore-forming fluid dominated by volcanic sulfur. The volcanic sulfur was either leached from the oceanic crust or sourced directly from the magmatic intrusion that is driving the hydrothermal circulation. The $\Delta^{33}S$ signatures of primary magmatic sulfur and leached rock sulfur

are likely indistinguishable, as neither reservoir contains significant amounts of photochemically-derived sulfur. The $\Delta^{33}S$ tool can therefore not be used to determine the relative contributions of these two sulfur sources, and independent methods, such as Se/S ratios must be applied (Huston et al., 1995).

The small range in $\Delta^{33}S$ values indicates a well-mixed source, suggesting that the sulfur was transported to the site of precipitation by the hydrothermal fluid, and there was no mixing with coeval surface sources. This suggests, therefore, that the seawater sulfate was incorporated into the hydrothermal fluid by a uniform process such as during recharge at the seafloor and transported through the hydrothermal system. The dissolved sulfate was abiotically reduced and mixed with reduced rock sulfur, forming a homogenized sulfur source in the hydrothermal fluid in the upflow zone, and ultimately at the site of subsurface sulfide precipitation.

The large magnitude (positive and negative), and range of $\Delta^{33}S$ values for the surface sulfides indicates multiple, non-homogenized sulfur sources, which may include the hydrothermal sulfur that formed the subsurface deposits. Larger $\Delta^{33}S$ values indicate lower contributions of hydrothermal-derived sulfur and higher contributions of local dissolved sulfate (negative $\Delta^{33}S$ values) or locally derived native sulfur (positive $\Delta^{33}S$ values). Contributions of non-hydrothermal sulfur directly form the water column would result in the incorporation of sulfur with $\Delta^{33}S$ compositions comparable to the most extreme positive and negative $\Delta^{33}S$ values recorded at Kidd Creek.

The sulfide turbidite samples, which represent collapsed vent chimneys, and have highly negative $\Delta^{33}S$ values, contain a large component of sulfur that was likely

directly reduced from sulfate in the water column. These turbidite horizons may also incorporate minor amounts of non-hydrothermal sulfide from the sediment or directly from the water column. These sulfides would likely have $\Delta^{33}S$ compositions comparable to the most extreme positive $\Delta^{33}S$ values recorded at Kidd Creek. Possible reductants include reduced iron from the hydrothermal fluid and organic carbon in the sediment. The $\delta^{34}S$ values of these samples range from 1.14 to 5.46 ‰, and are isotopically heavier than the massive sulfides, which is consistent with a reduced seawater sulfate source, relative to a volcanic-dominated source.

The positive $\Delta^{33}S$ values, for sulfide turbidites and sulfide-rich sinter, are interpreted to indicate that native sulfur (S_8) was reduced directly from the water column and incorporated into these surface hydrothermal sulfides, similar to the sulfide-rich sinter. Figure 9 illustrates the different sulfur reservoirs, with their associated $\Delta^{33}S$ values, that are relevant to Archean hydrothermal circulation.

The incorporation of sulfur from the surface environment at the discharge site suggests that the hydrothermal fluid was depleted in reduced sulfur, but not dissolved metals. The bulk of the reduced sulfur in the hydrothermal fluid precipitated in the subsurface. Excess dissolved metals that vented at the surface scavenged sulfur by chemical reduction of dissolved sulfate and native sulfur in the water column. Elevated $\Delta^{33}S$ values in surface hydrothermal sulfides in Archean terrains may be an indication of the proximity of significant massive sulfide that formed below the seafloor. These values may serve as an exploration vector when exploring for VMS deposits.

The most extreme $\Delta^{33}S$ values all correspond with regional sulfide-rich turbidites (i.e. hydrothermal vent sulfides that are distal to the main ore lenses and discharge region, but within the same host rock succession) (Fig. 8). These extreme values indicate that the sulfides that formed at these peripheral vent sites had a larger component of surface-derived sulfur than the sulfides formed above the massive sulfide lenses, at the main discharge site. This implies that the hydrothermal fluid venting at these sites is more depleted in reduced sulfur than the fluid venting at the main discharge site.

The most negative $\Delta^{33}S$ value recorded at Kidd Creek (-1.50‰ from a sulfide-rich turbidite) can be considered a minimum negative value for the Archean seawater sulfate reservoir. Using this value for seawater sulfate, and a $\Delta^{33}S$ value of 0 ‰ for volcanic sulfur, a simple mass-balance calculation can be performed to determine the relative contributions of these sources to the subsurface sulfide minerals at Kidd Creek. The average $\Delta^{33}S$ value for subsurface ore at Kidd Creek is -0.04 ‰ (± 0.03‰, 1σ), which results in a maximum contribution of ~3% seawater sulfate. Notably, estimates for modern hydrothermal systems range from 20 to 80% (Woodruff and Shanks, 1988; Humphris and Cann, 2000). The general mechanisms of ore formation in the Archean are thought to be similar to those of today (i.e. hydrothermal leaching of metals from the crust and reprecipitation of metals at seafloor discharge sites). Therefore, different environmental conditions in the Archean are the likely cause for the difference in sulfate-sulfur, compared to modern estimates. Lower concentrations of oceanic sulfate in the Archean (Habicht et al., 2002) may have resulted in a reduced contribution of seawater sulfate into the

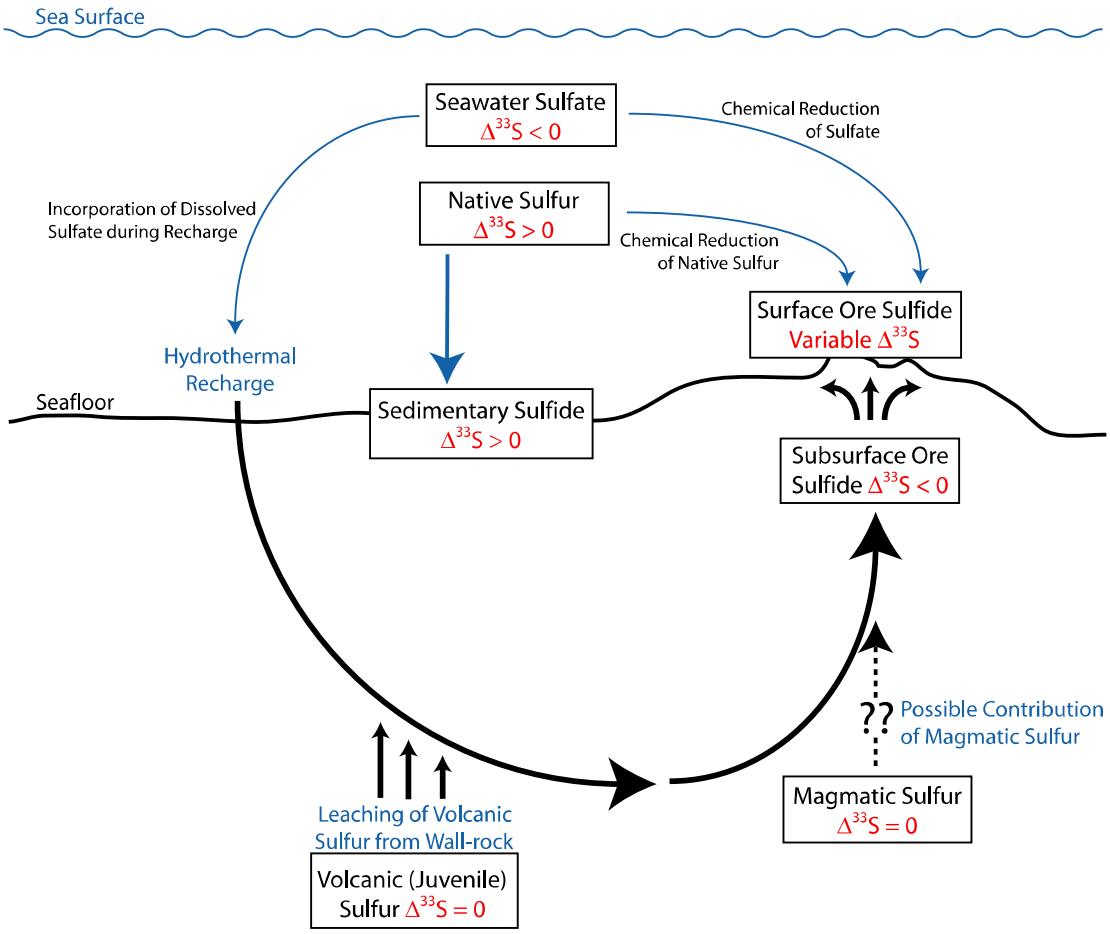

Figure 9: Conceptual diagram of surface sulfur reservoirs associated with seafloor hydrothermal circulation. Dissolved sulfate imparts a negative $\Delta^{33}S$ signature on the hydrothermal fluid. This signature is diluted towards 0‰ by addition of juvenile sulfur, and recorded in subsurface massive sulfides. A proportion of surface sulfur in surface ore sulfides is scavenged from coeval seawater sulfate and reduced sedimentary sulfide.

hydrothermal system, which led to a higher relative contribution of juvenile sulfur in the hydrothermal fluid at the discharge site. Higher heat flow in the Archean likely resulted in more vigorous hydrothermal circulation through the crust. It is unclear if increased circulation would affect the relative contributions of seawater sulfate and juvenile sulfur. Higher heat may have increased the ability of fluid to leach sulfur from the volcanic rock. However, the increased circulation would have also resulted in an increase drawdown of dissolved sulfate, which could counteract the increase in leached sulfur.

5.2 Isotopic Disequilibrium in Sulfide Mineral Pairs

The uses of $\Delta^{33}S$ values have been largely restricted to tracing the movement of sulfur between different Archean reservoirs. However, mass-independent fractionation of sulfur isotopes in the Archean provides a tool that, in certain geological environments, can be used to provide insights into the state of isotopic equilibrium between mineral pairs.

Isotopic equilibrium in mineral pairs is essential for isotope-thermometry calculations (Ohmoto and Rye, 1979). Suitability of mineral pairs for these calculations is often evaluated by the consistency of calculated temperatures with inferred geological conditions. If a temperature determined from a mineral pair is within an estimated temperature range, that temperature is assumed to be accurate, and the minerals in the pair are assumed to be in isotopic equilibrium, which may not necessarily be a correct assumption. This reasoning is circular and other tests are needed. A simple graphical test can be used to determine what mineral pairs are consistent with equilibrium in a sample set with mass-independent fractionation, such

as the Kidd Creek sample set. The use of $\Delta^{33}S$ values provides an independent tool that can be used to identify pairs that are not in equilibrium, even though their calculated temperatures appear to be reasonable.

Equilibrium in a multiple-isotope system with at least one source that is not on the terrestrial fractionation line leads to the development of a secondary fractionation array that is parallel to the reference mass-fractionation line (Fig. 10) (Matsuhisa et al., 1978). In the sulfur multiple-isotope system, this secondary array would define a constant value of $\Delta^{33}S$. Therefore, for two minerals to be in isotopic equilibrium they must have similar $\Delta^{33}S$ values. Although the same $\Delta^{33}S$ value is a necessary condition for isotopic equilibrium, it is not sufficient, and common $\Delta^{33}S$ values could instead indicate a shared sulfur source. However, dissimilar $\Delta^{33}S$ values clearly indicate isotopic disequilibrium between minerals.

The isotopic compositions of the mineral pairs are plotted on a $\Delta^{33}S$ vs. $\delta^{34}S$ graph (Fig. 11). The relative differences in $\delta^{34}S$ values within the sulfide pairs are generally consistent with predicted equilibrium fractionations between sulfide minerals ($\delta^{34}S_{Gn} < \delta^{34}S_{Bn} < \delta^{34}S_{Ccp} < \delta^{34}S_{Sp} \approx \delta^{34}S_{Po} < \delta^{34}S_{Py}$) (Ohmoto, 1986). The $\Delta^{33}S$ values, however, provide a more accurate indication of the state of equilibrium between two minerals. In Figure 11, mineral pairs with $\Delta^{33}S$ values that are within 0.04 per mil of each other are consistent with isotopic equilibrium.

Of the five mineral pairs analyzed from the north orebody, only pairs #6 and #7 have $\Delta^{33}S$ relationships that clearly indicate disequilibrium. Pairs #3, #4 and #5 have $\Delta^{33}S$ values that overlap, and are consistent with equilibrium.

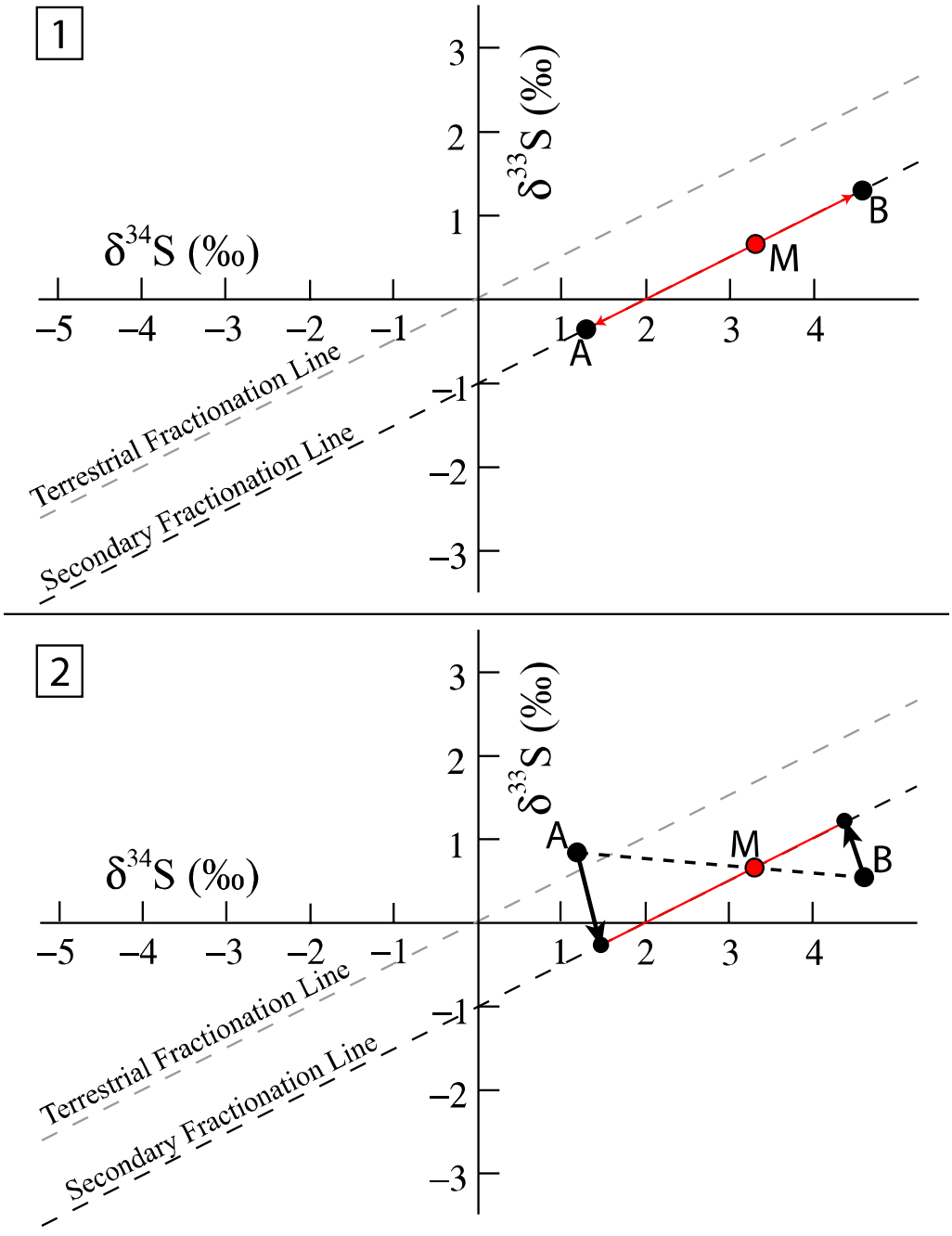

Figure 10: Three isotope plots of system with bulk composition M and minerals A and B. 1: The isotopic composition of minerals A and B precipitating in equilibrium from a fluid with a composition M. Minerals A and B will fall on a common fractionation line with a slope parallel to the terrestrial fractionation line, resulting in similar $\Delta^{33}S$ values. 2: The isotopic composition of minerals A and B (with different initial $\Delta^{33}S$ values) will shift towards a secondary fractionation line during as they equilibrate.

Equilibrium fractionation between sphalerite and pyrrhotite is negligible, and pyrrhotite-sphalerite mineral pairs in equilibrium should have similar $\delta^{34}S$ values. Pairs #4 and #5 have $\delta^{34}S$ values that are within analytical uncertainty of each other whereas pair #6 does not. These results are consistent with the equilibrium relationships defined by $\Delta^{33}S$ values. For pyrrhotite-sphalerite pairs, and other mineral pairs with negligible equilibrium fractionation factors (such as millerite-sphalerite; Ohomoto and Rye, 1979), $\Delta^{33}S$ values provide the only isotopic evidence for the state of equilibrium between the two minerals.

The disequilibrium relationship indicated by $\Delta^{33}S$ values for the sphalerite-pyrite pair (#7) is consistent with the $\delta^{34}S$ relationship between the two minerals. The pyrite in pair #7 is isotopically lighter than the sphalerite (Fig. 11). Under equilibrium conditions, pyrite should have a more positive $\delta^{34}S$ value than sphalerite (Ohmoto and Rye, 1986). A paleotemperature can therefore not be calculated using this pair.

Galena and pyrite have the largest fractionation under equilibrium conditions, relative to the other major sulfides analyzed, making this mineral pair ideal for paleothermometric calculations. The $\Delta^{33}S$ values for this pair indicate consistency with equilibrium. The $\delta^{34}S$ values are also consistent with equilibrium fractionation, and yield a calculated temperature of 213 degrees Celsius (± 35°C). This value is consistent with temperatures predicted by Hannington et al. (1999a) for sulfide precipitation in the massive sulfide lens, based on temperature-solubility models. The $\Delta^{33}S$ relationships for the two bornite-chalcopyrite mineral pairs (#s 1 and #2) from the high-grade bornite zone are consistent with equilibrium. The bornite is

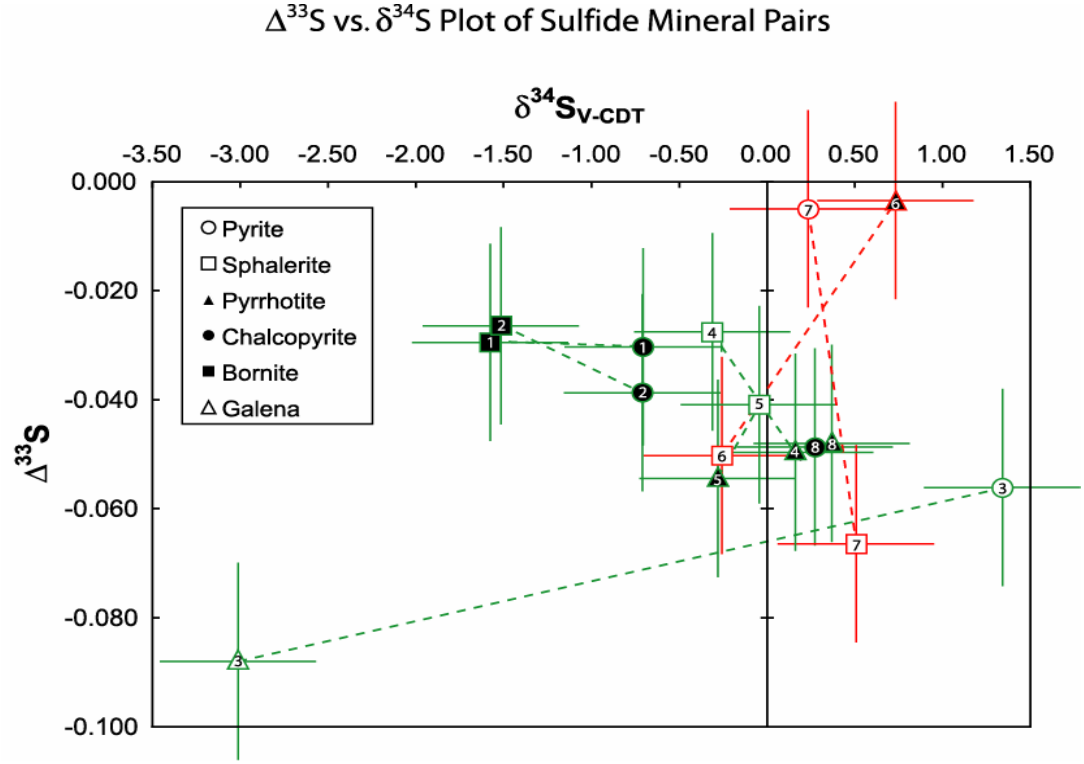

Figure 11: Sulfur multiple-isotope measurements for mineral pairs from Kidd Creek. Pairs are numbered and connected by broken tie-lines. Pairs in isotopic disequilibrium (colored in red) have tie lines that are not in experimental reproducibility of being parallel to the x-axis. Tie-lines that are parallel to the x-axis indicate consistency with isotopic equilibrium (colored in green). Pairs #6 and #7 are in isotopic disequilibrium. The other six pairs have $\Delta^{33}S$ values that are consistent with equilibrium. Error bars indicate 2σ uncertainties.

thought to have formed by replacement of chalcopyrite. The similar $\Delta^{33}S$ values suggest that both minerals have the same sulfur source and replacement of chalcopyrite by bornite involved addition of copper, but not sulfur. The difference in $\delta^{34}S$ values for the separate minerals in each pair yield paleotemperatures of 209 degrees Celsius (± 234˚C) for pair #1 and 227 degrees Celsius (± 245˚C) for pair #2. These temperatures are consistent with temperatures calculated using independent methods (Hannington et al, 1999a), which is further support of an equilibrium relationship between these minerals. The large errors in calculated temperatures are due to the small equilibrium fractionation between bornite and chalcopyrite.

The isotopic compositions of the chalcopyrite-pyrrhotite pair (#8), from the copper stringer zone below the central orebody, plot within error of each other. The $\Delta^{33}S$ values are consistent with isotopic equilibrium. Equilibrium isotopic thermometry calculations are equivocal for this pair, and cannot bear on the inferences based on $\Delta^{33}S$ values. We note that similar $\Delta^{33}S$ values are not sufficient indicators for isotopic equilibrium as similar $\Delta^{33}S$ values in mineral pairs can also be caused by the minerals having the same sulfur source. It is not clear whether the results from pair #8 reflect this situation, or whether they reflect the relative imprecision of our $\delta^{34}S$ measurements.

Chapter 6: Conclusions

The focused study of multiple sulfur isotope compositions of sulfides at the Kidd Creek VMS deposit has demonstrated the use of atmospheric mass-independent sulfur signatures as a tracer of the movement of sulfur, from different surface reservoirs, through a seafloor hydrothermal system. Sulfur from seawater sulfate will have a negative $\Delta^{33}S$ value, sulfur from sedimentary sulfide will have a positive $\Delta^{33}S$ value, and juvenile sulfur has a $\Delta^{33}S$ value of 0 ‰.

The sulfide ores at Kidd Creek can be grouped based on $\Delta^{33}S$ values into two environments of precipitation: subsurface ore, consisting of massive sulfide lenses, a Cu-rich stringer zone and disseminated wall-rock sulfides, and surface sulfides, which consist of sulfide-rich sinter and turbidites. The $\Delta^{33}S$ values of the subsurface ore show little variability, indicating a homogenous sulfur source. The $\Delta^{33}S$ values are slightly negative, indicating a minor component of sulfur from seawater sulfate in the hydrothermal fluid. This sulfate was transported through the hydrothermal system and was reduced by reactions with the wall rock. The majority of the reduced sulfur in the hydrothermal fluid was leached from sulfides in the volcanic rocks. A component of sulfur from magmatic fluids may be incorporated into the hydrothermal fluid.

The surface sulfides have a wide range of positive and negative $\Delta^{33}S$ values, indicating multiple sources of sulfur, which is in contrast to the single, homogenized source for the subsurface sulfur. Large negative $\Delta^{33}S$ values indicate the reduction of

sulfur directly from seawater sulfate. Large positive values indicate remobilization and incorporation of sedimentary sulfur during precipitation of hydrothermal sulfides. A vent fluid that is depleted in reduced sulfur, but not dissolved metals, resulted in the stripping of sulfur from the surface environment to precipitate metal sulfides. A large surface sulfur signature may indicate the presence of significant subsurface sulfide mineralization, and could be used as a potential exploration tool for VMS deposits.

Using the most negative $\Delta^{33}S$ value as an estimate for the mass-independent signature of the Archean ocean sulfate reservoir, a mass-balance of a two component system (volcanic sulfur and seawater sulfate) for the subsurface sulfides results in a ~3% contribution of seawater sulfate to the otherwise volcanic sulfur-dominated hydrothermal fluid. This value is much lower than estimates of sulfate contributions for modern hydrothermal systems, and may be a result of lower oceanic sulfate concentrations in the Archean.

Sulfur multiple-isotope measurements also provide a natural reference frame to evaluate isotopic disequilibrium between sulfide mineral pairs. When minerals are in equilibrium, $\Delta^{33}S$ values are similar; minerals in isotopic disequilibrium may have different $\Delta^{33}S$ values. This isotopic test for disequilibrium provides a criterion for the suitability of mineral pairs for paleothermometry calculations that is independent of conventional methods for evaluating disequilibrium. A unique benefit of the technique is that it can be used to evaluate isotopic disequilibrium between minerals with negligible equilibrium fractionation factors.

Results of evaluations of $\Delta^{33}S$ values as a test for disequilibrium in mineral pairs from the Kidd Creek VMS deposit are consistent with $\delta^{34}S$ values. Isotopic analyses of sulfide mineral pairs from Kidd Creek mostly indicate equilibrium conditions. Pairs that are clearly out of equilibrium, based on $\delta^{34}S$ values, are also demonstrated to be in disequilibrium, when their $\Delta^{33}S$ values are compared. The overriding utility of this method is its use to determine disequilibrium in pairs that appear to be in equilibrium based on $\delta^{34}S$ values and textural evidence.

This technique for evaluating isotopic disequilibrium has some profound implications for Archean ore deposits with multiple sources of sulfur. These isotopic conditions can be used to verify the suitability of mineral pairs for paleothermometric calculations, and has the potential to delineate different ore forming events in a single ore deposit. This technique can also be used to examine the sources and emplacement mechanisms of sulfur in diverse Archean ore-forming environments, such as nickel sulfide accumulations in komatiites, detrital gold-uranium deposits and banded iron formation-hosted gold deposits.

Appendix

Calculation of uncertainty in $\Delta^{33}S$ using uncertainties of $\delta^{33}S$ and $\delta^{34}S$

$$\Delta^{33}\mathrm{S} = \delta^{33}\mathrm{S} - \left[\left(\frac{\delta^{34}\mathrm{S}}{1000} + 1\right)^{\lambda_{\mathrm{RFL}}} - 1\right] \times 1000$$

$$\sigma^2_{\Delta^{33}S} = \left(\frac{\partial \Delta^{33}S}{\partial \delta^{33}S}\right)^2 \sigma^2_{\delta^{33}S} + \left(\frac{\partial \Delta^{33}S}{\partial \delta^{34}S}\right)^2 \sigma^2_{\delta^{34}S} + \left[\sigma_{\delta^{33}S}\sigma_{\delta^{34}S}\left(\frac{\partial \Delta^{33}S}{\partial \delta^{33}S}\right)\left(\frac{\partial \Delta^{33}S}{\partial \delta^{34}S}\right)\right]$$

Assumption: Covariance of $\delta^{33}S$ and $\delta^{34}S = 0$

$$\therefore \left[\sigma_{\delta^{33}S}\sigma_{\delta^{34}S}\left(\frac{\partial \Delta^{33}S}{\partial \delta^{33}S}\right)\left(\frac{\partial \Delta^{33}S}{\partial \delta^{34}S}\right)\right] = 0$$

$$\frac{\partial \Delta^{33}S}{\partial \delta^{33}S} = 1 \qquad \sigma_{\delta^{33}S} = 0.11‰ \qquad \sigma_{\delta^{34}S} = 0.22‰$$

$$\frac{\partial \Delta^{33}S}{\partial \delta^{34}S} = -\lambda\left(\frac{\delta^{34}S}{1000} + 1\right)^{\lambda - 1} \approx -0.515 \text{ for range of observed } \delta^{34}S \text{ values}$$

The uncertainty in $\Delta^{33}S$, calculated by the propagation of uncertainties in $\delta^{33}S$ and $\delta^{34}S$ values results in an uncertainty of $\sigma = 0.158‰$. Covariance between $\delta^{33}S$ and $\delta^{34}S$ results in an uncertainty of $\sigma = 0.009‰$.

Results of measurements of internal standard, P1 (Pyrite) for analytical uncertainty determination:

$\delta^{33}S$	$\delta^{34}S$	$\delta^{36}S$	$\Delta^{33}S$	$\Delta^{36}S$
-1.03	-1.99	-4.84	-0.01	-0.72
-1.09	-2.06	-4.44	-0.03	-0.22
-1.04	-2.00	-4.85	-0.01	-0.72
-1.08	-2.10	-5.51	0.00	-1.15
-1.35	-2.64	-6.15	0.01	-0.72
-1.05	-2.03	-4.55	-0.01	-0.38
-1.24	-2.38	-5.87	-0.01	-0.94
-1.17	-2.27	-5.64	-0.01	-0.94
-1.21	-2.33	-5.66	-0.01	-0.84
-1.25	-2.41	-5.86	-0.01	-0.89

Bibliography

Alt, J.C., 1999, Hydrothermal alteration and mineralization of oceanic crust: mineralogy, geochemistry, and processes: Volcanic-Associated Massive Sulfide Deposits: Processes and Examples in Modern and Ancient Settings. Reviews in Economic Geology, v. 8, Barrie, C.T. and Hannington, M.D. (eds.), p. 133-155.

Barrie, C.T., 1999, Komatiite flows of the Kidd Creek Footwall, Abitibi Subprovince, Canada: The Giant Kidd Creek Volcanogenic Massive Sulfide Deposit, Western Abitibi Subprovince, Canada. Economic Geology Monographic 10, Hannington, M.D. and Barrie, C.T. (eds.), p. 143-161.

Barrie, C.T., and Hannington, M.D., 1999, Classification of volcanic-associated massive sulfide deposits based on host-rock composition: Volcanic-Associated Massive Sulfide Deposits: Processes and Examples in Modern and Ancient Settings. Reviews in Economic Geology, v. 8, Barrie, C.T. and Hannington, M.D. (eds.), p. 1-11.

Barrie, C.T., Hannington, M.D., and Bleeker, W, 1999, The giant Kidd Creek volcanic-associated massive sulfide deposit, Abitibi Subprovince, Canada: Volcanic-Associated Massive Sulfide Deposits: Processes and Examples in Modern and Ancient Settings. Reviews in Economic Geology, v. 8, Barrie, C.T. and Hannington, M.D. (eds.), p. 247-259.

Bekker, A., Holland , H.D., Wang, P.L., et al., 2004, Evolution of the early precambrian atmosphere, climatic changes, and the rise of atmospheric oxygen: Abstracts of Papers of the American Chemical Society 228: U700.

Bleeker, W., and Parrish, R.R., 1996, Stratigraphy and U-Pb zircon geochronology of Kidd Creek: Implications for the formation of giant volcanogenic massive sulphide deposits and the tectonic history of the Abitibi greenstone belt: Canadian Journal of Earth Sciences, v. 33, p. 1213-1231.

Bleeker, W., 1999, Structure, stratigraphy, and primary setting of the Kidd Creek volcanogenic massive sulfide deposit: A semiquantitative reconstruction: The Giant Kidd Creek Volcanogenic Massive Sulfide Deposit, Western Abitibi Subprovince, Canada. Economic Geology Monographic 10, Hannington, M.D. and Barrie, C.T. (eds.), p. 71-121.

Canfield, D.E., and Raiswell, R., 1999, The Evolution of the sulfur cycle: American Journal of Science, v.299, p. 697-723.

Corfu, F., 1993, The evolution of the southern Abitibi greenstone belt in light of precise U-Pb geochronology: Economic Geology, v. 88, p. 1323-1341.

Edmond, J.M., Measures, C., Mangum, B., Sclater, F.R., Collier, R., and Hudson, A., 1979, On the formation of metal-rich deposits at ridge crests: Earth and Planetary Science Letters, v. 46, p. 19-30.

Farquhar, J., Chacko, T., and Frost, B.R., 1993, Strategies for high-temperature oxygen isotope thermometry: a worked example from the Laramie Anorthosite Complex, Wyoming, USA: Earth and Planetary Science Letters, v. 117, p. 407-422.

Farquhar, J., Bao, H.M., and Thiemens, M., 2000, Atmospheric influence of Earth's earliest sulfur cycle: Science, v. 289 (5480), p. 756-758.

Farquhar, J., Savarino, J., Airieau, S., Thiemens, M.H., 2001, Observation of wavelength-sensitive mass-independent sulfur isotope effects during SO_2 photolysis: Implications for the early atmosphere: Journal of Geophysical Research, v. 160, p. 32829-32839.

Farquhar, J., and Wing, B.A., 2003, Multiple sulfur isotope analyses: Applications in geochemistry and cosmochemistry: Earth and Planetary Science Letters, v. 213, p. 1-13.

Franklin, J.M., Sangster, D.M., and Lydon, J.W., 1981, Volcanic associated massive sulphide deposits: Economic Geology 75th Anniversary Volume; pp. 485-627.

Gao, X, and Thiemens, M.H., 1991, Systematic study of sulfur isotopic composition in iron meteorites and the occurrence of excess ^{33}S and ^{36}S: Geochimica et Cosmochimica Acta, v. 55, p. 2671–2679.

Gibson, H., Morton, R.L., and Hudak, G.J., 1999, Submarine volcanic processes, deposits, and environments favorable for the location of volcanic-associated massive sulfide deposits: Volcanic-Associated Massive Sulfide Deposits: Processes and Examples in Modern and Ancient Settings. Reviews in Economic Geology, v. 8, Barrie, C.T. and Hannington, M.D. (eds.), p. 13-51.

Habicht, K.S., Gade, M., Thamdrup, B., Berg, P., and Canfield, D.E., 2002, Calibration of Sulfate Levles in the Archean Ocean: Science, v. 298, p. 2372-2374.

Hannington, M.D., Bleeker, W. and Kjarsgaard, I., 1999a, Sulfide mineralogy, geochemistry, and ore genesis of the Kidd Creek deposit: Part I. North, central and south orebodies: The Giant Kidd Creek Volcanogenic Massive Sulfide Deposit, Western Abitibi Subprovince, Canada. Economic Geology Monographic 10, Hannington, M.D. and Barrie, C.T. (eds.), p. 163-224.

Hannington, M.D., Bleeker, W. and Kjarsgaard, I., 1999b, Sulfide mineralogy, geochemistry, and ore genesis of the Kidd Creek deposit: Part II. The bornite zone: The Giant Kidd Creek Volcanogenic Massive Sulfide Deposit, Western Abitibi Subprovince, Canada. Economic Geology Monographic 10, Hannington, M.D. and Barrie, C.T. (eds.), p. 225-266.

Hu, Guixing, Rumble, D., and Wang, Pei-Ling, 2003, An ultraviolet laser microprobe for the in situ analysis of multisulfur isotopes and its use in measuring Archean sulfur isotope mass-independent anomalies: Geochimica et Cosmochimica Acta, v. 67, p. 3101–3117.

Hulston, J.R., and Thode, H.G., 1965, Variations in ^{33}S, ^{34}S and ^{36}S contents of meteorites and their relation to chemical and nuclear effects: Journal of Geophysical Research, v. 70 (14), p. 3475-3484.

Humphres, S.E., and Cann, J.R., 2000, Constraints on the energy and chemical balances of the modern TAG and ancient Cyprus seafloor sulfide deposits: Journal of Geophysical Research, Solid Earth, v. 105 (B12), 28477-28488.

Huston, D.L, 1999, Stable isotopes and their significance for understanding the genesis of volcanic-hosted massive sulfide deposits: a review: Volcanic-Associated Massive Sulfide Deposits: Processes and Examples in Modern and Ancient Settings. Reviews in Economic Geology, v. 8, Barrie, C.T. and Hannington, M.D. (eds.), p. 157-179.

Huston, D.L., Brauhart, C.W., Drieberg, S.L., et al., 2001, Metal leaching and inorganic sulfate reduction in volcanic-hosted massive sulfide mineral systems: Evidence from the paleo-Archean Panorama district, Western Australia: Geology, v. 29 (8), p. 687-690.

Huston, D.L., and Taylor, B.E., 1999, Genetic significance of oxygen and hydrogen isotope variations at the Kidd Creek volcanic-hosted massive sulfide deposit, Ontario, Canada: The Giant Kidd Creek Volcanogenic Massive Sulfide Deposit, Western Abitibi Subprovince, Canada. Economic Geology Monographic 10, Hannington, M.D. and Barrie, C.T. (eds.), p. 335-350.

Huston, D.L, Sie, S.H., Cooke, DH., Both, R.A., and Suter, G.F., 1995, Trace elements in sulfide minerals from eastern Australian volcanic-hosted massive sulfide deposits: Part II. Selenium levels in pyrite: Comparison with $\delta^{34}S$ values and implications for the source of sulfur in volcanogenic hydrothermal systems: Economic Geology, v. 90, p. 1185-1196.

Jackson, S.L., and Cruden, A.R., 1995, Formation of the Abitibi greenstone belt by arc-trench migration: Geology, v. 23, p. 471-474.

Koopman, E.R., Hannington, M.D., Santaguida, F., and Cameron, B.I., 1999, Petrology and geochemistry of proximal hydrothermal alteration in the Mine Rhyolite at Kidd Creek: The Giant Kidd Creek Volcanogenic Massive Sulfide Deposit, Western Abitibi Subprovince, Canada. Economic Geology Monographic 10, Hannington, M.D. and Barrie, C.T. (eds.), p. 267-296.

Kretz, R., 1983, Symbols for rock-forming minerals: American Mineralogist, v. 68 (1-2), p. 277-279.

Krouse, H.R., and Coplen, T.B., 1997, Reporting of relative sulfur isotope-ratio data: Pure and Applied Chemistry, v. 69 (2), p. 293-295.

Langford, F.F., and Morin, J.A., 1976, The development of the Superior province of northwestern Ontario by merging island arcs: American Journal of Science, v. 276, p. 1023-1034.

Ludden, J.N., and Hubert, C., 1986, Geologic evolution of the Late Archean Abitibi greenstone belt of Canada: Geology, v. 14, p. 707-711.

Matsuhisa, Y., Goldsmith, J.R., and Clayton, R.N., 1978, Mechanisms of hydrothermal crystallization of quartz at 250°C and 15 kbar: Geochimica et Cosmochimica Acta, v.42, p. 173-182.

Mojzsis, S.J., Coath, CD, and Greenwood, J.P., 2003, Mass-independent isotope effects in Archean (2.5 to 3.8 Ga) sedimentary sulfides determined by ion microprobe analysis: Geochimica et Cosmochimica Acta, v. 67 (9), p. 1635-1658.

Ohmoto, H., 1986, Stable isotope geochemistry of ore deposits: In: Reviews in Mineralogy, v. 16, Stable isotopes in high temperature geological processes, Valley, J.W., Taylor, H.P.Jr., and O'neil, J.R., (eds.), p. 491-505.

Ohmoto, H., 1992, Biogeochemistry of sulphur and the mechanisms of sulphide-sulphate mineralization in Archaean oceans: In: Schidlowski, M., Golubic, Sl, Kimberly, M.M., McKirdy, D.M., Trudinger, P.D. (Eds.), Early Organic Evolution. Springer-Verlag, Berlin, Heidelberg, New York, pp. 378-397.

Ohmoto, H., 1996, Formation of volcanogenic massive sulfide deposits: The Kuroko perspective, Ore Geology Reviews, v. 10, p. 135-177.

Ohmoto, H., and Rye, R.O., 1979, Isotopes of sulfur and carbon: Geochemistry of Hydrothermal Ore Deposits, Second Edition, Barnes, H.L. (ed.), p. 509-567.

Ohmoto, H., and Skinner, B.J. (Editors), 1983, The Kuroko and related volcanogenic massive sulfide deposits: Economic Geology Monograph 5, p. 604.

Ono, S., Eigenbrode, J.L., Pavlov, A.A., Kharecha, P., Rumble, D., Kasting, J.F., Freeman, K.H., 2003, New insights into Archean sulfur cycle from mass-independent sulfur isotope records from the Hamersley Basin, Australia: Earth and Planetary Science Letters, v. 213, p. 15-30.

Pavlov, A.A., and Kasting, J.F., 2002, Mass-independent fractionation of sulfur isotopes in Archean sediments: Strong evidence for an anoxic Archean atmosphere: Astrobiology, v. 2 (1), p. 27-41.

Pottorf, R.J., and Barnes, H.L., 1983, Mineralogy, geochemistry, and ore genesis of hydrothermal sediments from the Atlantis II deep, Red Sea: Economic Geology Monograph 5, p. 198-223.

Prior, B.J., Gibson, H.L., Watkinson, D.H., and Cook, R.E., 1999, Anatomy, lithogeochemistry, and emplacement mechanisms for the QP Rhyolite, Kidd Creek Mine, Timmins, Ontario: The Giant Kidd Creek Volcanogenic Massive Sulfide Deposit, Western Abitibi Subprovince, Canada. Economic Geology Monographic 10, Hannington, M.D. and Barrie, C.T. (eds.), p. 123-142.

Rumble, D., Hoering, T.C., Palin, J.M., 1993, Preparation of SF_6 for sulfur isotope analysis by laser-heating sulfide minerals in the presence of F_2 gas: Geochimica et Cosmochimica Acta, v. 57 (18), p. 4499-4512.

Sangster, D.F., 1968, Relative sulphur isotope abundances of ancient seas and strata-bound sulphide deposits: Geological Association of Canada Proceedings, v. 19, p. 79-91.

Shanks, W.C., 2001, Stable Isotopes in Seafloor Hydrothermal Systems: Vent fluids, hydrothermal deposits, hydrothermal alteration, and microbial processes: Stable Isotope Geochemistry, Reviews in Mineralogy and Geochemistry, v. 43, Valley, J.W. and Cole, R. (eds.), p. 469-517.

Shanks, W.C., and Seyfried, W.E., Jr., 1987, Stable isotope studies of vent fluids and chimney minerals, southern Juan de Fuca Ridge: Sodium metasomatism and seawater sulfate reduction: Journal of Geophysical Research, v. 92, p. 11387-11399.

Smith, J.W., 2000, Isotopic fractionations accompanying sulfur hydrolysis: Geochemical Journal, v. 34, p. 95-99.

Strauss, H., 1989, Carbon and sulfur isotope data for carbonaceous metasediments from the Kidd Creek massive sulfide deposit and vicinity, Timmins, Ontario: Economic Geology, v. 84, p. 959-962.

Strauss, H., 2003, Sulphur isotopes and the early Archaean sulphur cycle: Precambrian Research, v. 126, p. 349-361.

Thiemens, M.H., 1999, Atmospheric Science – Mass-independent isotope effects in planetary atmospheres and the early solar system: Science, v. 283, p. 341-345.

Walker, J.C.G., and Brimblecombe, P., 1985, Iron and Sulfur in the pre-biological ocean: Precambrian Research, v. 28 (3-4), p. 205-222.

Wing, B.A., Farquhar, J., Rumble, D., Valley, J.W., 2002, $\Delta^{33}S$ evidence from superior province ore deposits for a sulfate-stratified ocean at 2.7 Ga: Abstracts with Programs 34, Geological Society of America, 2002, p. 516.

Woodruff, L.G., and Shanks, W.C., 1988, Sulfur isotope study of chimney minerals and vent fluids from 21-degrees-N, East Pacific Rise – Hydrothermal sulfur sources and disequilibrium sulfate reduction: Journal of Geophysical Research, Solid Earth and Planets, v. 93 B5), 4562-4572.

Vearncombe, S., Barley, M.E., Groves, D.I., McNaughton, N.J., Mikucki, E.J., and Vearncombe, J.R., 1995: 3.26 Ga black smoker-type mineralization in the Strelley belt, Pilbara craton, Western Australia: Geological Society of London Journal, v. 152, p. 587-590.

Yang, K., and Scott, S.D., 1996, Possible contribution of a metla-rich magmatic fluid to a seafloor hydrothermal system: Nature, v., 383, p. 420-423.